ISSN 1075-7015, Geology of Ore Deposits, 2016, Vol. 58, No. 4, pp. 284–307. © Pleiades Publishing, Ltd., 2016.
Original Russian Text © Yu.N. Nikolaev, I.A. Baksheev, V.Yu. Prokofiev, E.V. Nagornaya, L.I. Marushchenko, Yu.N. Sidorina, A.F. Chitalin, I.A. Kal'ko, 2016, published in Geologiya Rudnykh Mestorozhdenii, 2016, Vol. 58, No. 4, pp. 319–345.

Gold–Silver Mineralization in Porphyry–Epithermal Systems of the Baimka Trend, Western Chukchi Peninsula, Russia

Yu. N. Nikolaev[a], I. A. Baksheev[a], V. Yu. Prokofiev[b], E. V. Nagornaya[c], L. I. Marushchenko[a], Yu. N. Sidorina [a], A. F. Chitalin[d], and I. A. Kal'ko[a]

[a] *Geological Faculty, Moscow State University, Moscow, 119991 Russia*
[b] *Institute of Geology of Ore Deposits, Petrography, Mineralogy, and Geochemistry, Russian Academy of Sciences, Staromonetnyi per. 35, Moscow, 119017 Russia*
[c] *Institute of Geochemistry and Analytical Chemistry, ul. Kosygina 19, Moscow, 119991 Russia*
[d] *Regional Mining Company LLC, ul. Sadovnicheskaya 4, Moscow, 115035 Russia*

Received July 22, 2015

Abstract—Mineralogical, fluid inclusion, and geochemical studies of precious metal mineralization within the Baimka trend in the western Chukchi Peninsula have been preformed. Porphyry copper–molybdenum–gold deposits and prospects of the Baimka trend are spatially related to monzonitic rocks of the Early Cretaceous Egdygkych Complex. Four types of precious metal-bearing assemblages have been identified: (1) chalcopyrite + bornite + quartz with high-fineness native gold enclosed in bornite, (2) low-Mn dolomite + quartz + sulfide (chalcopyrite, sphalerite, galena, tennantite-tetrahedrite) ± tourmaline with low-fineness native gold and hessite, (3) rhodochrosite + high-Mn dolomite + quartz + sulfide (chalcopyrite, sphalerite, galena, tennantite-tetrahedrite) with low-fineness native gold, electrum, acanthite, Ag and Au–Ag tellurides, and Ag sulfosalts, and (4) calcite + quartz + sulfide (chalcopyrite, sphalerite, galena) with low-fineness native gold, Ag sulfides and selenides, and Ag-bearing sulfosalts. Study of fluid inclusions from quartz, sphalerite, and fluorite have revealed that hydrothermal ores within the Baimka trend precipitated from fluids with strongly variable salinity at temperatures and pressures ranging from 594 to 104°C and from 1200 to 170 bar, respectively. An indicator of vertical AgPbZn/CuBiMo geochemical zoning is proposed. The value range of this indicator makes it possible to estimate the erosion level of the porphyry–epithermal system. The erosion level of the Baimka deposits and prospects deepens in the following order: Vesenny deposit → Pryamoi prospect → Nakhodka prospect → Peschanka deposit → III Vesenny prospect.

DOI: 10.1134/S107570151604005X

INTRODUCTION

Precious metal mineralization (Au, Ag, PGE) is typical of porphyry copper–molybdenum deposits (Sillitoe, 2010). At some porphyry deposits, the gold reserves are giantic, e.g., Pebble, US (3050 t of gold) and Grasberg, Indonesia (2900 t of gold). Some deposits have elevated Pd contents (Santo Tomas II, Philippines; Elatsite, Bulgaria; Bozshakol, Kazakhstan; Kalmakyr, Uzbekistan). (Tarkian, Koopman, 1995; Tarkian et al., 2003; Pašava et al., 2010).

According to the general model of porphyry deposits reported by Sillitoe (2010), gold mineralization is localized immediately in and beyond the copper stockwork. In the second case, it belongs to the HS (high sulfidation) and IS (intermediate sulfidation) epithermal types and subepithermal (transitional) carbonate–base-metal ore; it is also accompanied by Ag minerals. Within the copper stockwork, gold is associated with bornite and chalcopyrite; minerals associated with gold in the epithermal ores are identical to those in proper epithermal deposits (galena, sphalerite, chalcopyrite, enargite, tennantite–tetrahedrite, goldfieldite, acanthite, hessite, stützite, sylvanite); in subepithermal ores, gold is associated with galena, sphalerite, tennantite-tetrahedrite, chalcopyrite, hessite, petzite, and stützite (LeFort et al., 2011).

This article focuses on the mineral assemblages and geochemical features of precious metal mineralization within the Baimka trend including large porphyry Cu–Mo–Au deposit Peschanka and some smaller deposits and prospects.

Corresponding author: V.Yu. Prokofiev. E-mail: vpr@igem.ru

GEOLOGY OF THE BAIMKA TREND

The Baimka trend is located in the southeastern part of the Anyui Upland within a flattened low-hill terrain divided by streams of the drainage area of the Bol'shoi Anyui River. The near-meridional striking Baimka trend extends for 90 km and is related to a system of large NW-trending, predominantly dextral

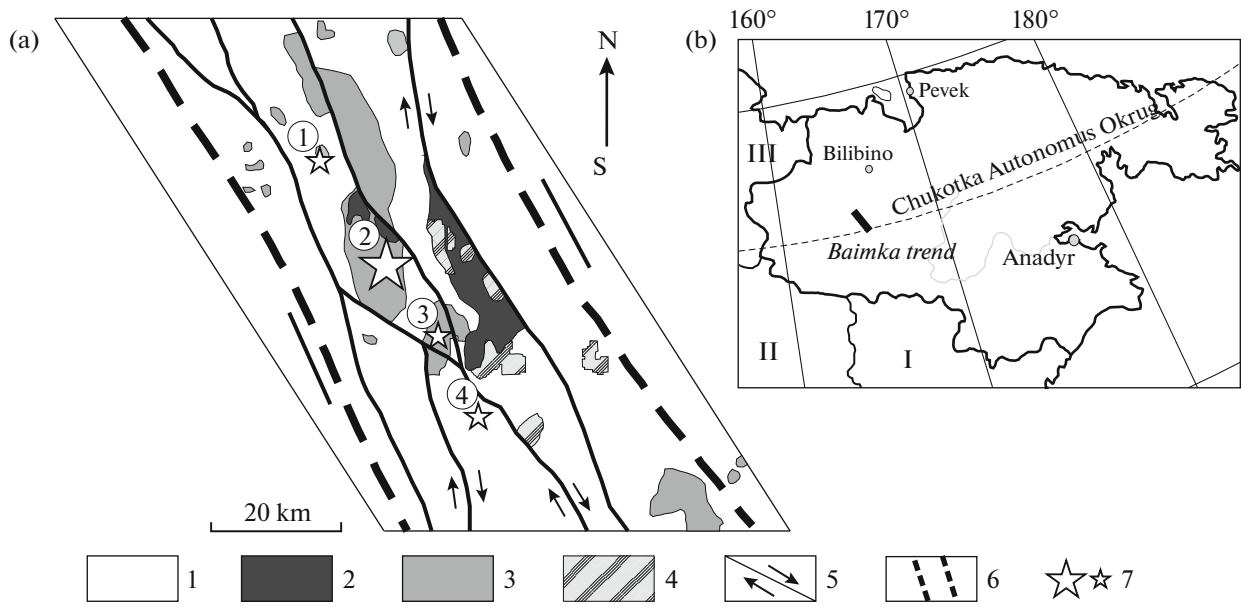

Fig. 1. Structure (a) and geographical location (b) of Baimka trend. (I) Kamchatka krai, (II) Magadan Oblast, (III) Sakha (Yakutia) Republic. (1) Fold–thrust Paleozoic to Mesozoic complex, (2) Lower Cretaceous volcanic and volcanic terrigenous sediments, (3) Early Cretaceous Egdykgych Complex, (4) Late Cretacous Omchak Complex, (5) dextral strike slip faults, (6) outlines of Baimka trend, (7) porphyry copper–molybdenum deposits and prospects. Numerals in circles: (1) Omchak ore field, (2) Peschanka ore field, (3) Nakhodka ore field, (4) Omchak ore field.

strike slips of Early Cretaceous age (Chitalin et al., 2013) (Fig. 1). Meridional faults and detachments governing ore stockworks of porphyry copper deposits, NE-trending left lateral strike slips and strike-slip faults, and gentle thrusts (in 2013, boreholes in the Egdykgych Valley transected the fault along which monzodiorite are thrust onto carbonaceous terrigenous sediments of the Early Cretaceous Ainakhkurgen Formation) are conjugate with the main strike slips. The described area comprises Early Jurassic tuff–terrigenous sediments, forming large brachyanticline slightly extended NNE; Early Cretaceous volcanic and volcanic terrigenous rocks surround this brachyanticline.

Ultramafics of the Early Triassic Aluchin Complex composing the Aluchin Rise are probably allochtonous and are early intrusion rocks.

The Late Jurassic volcanic sedimentary sequence is intruded by bodies of the Baimka, Egdykgych, and Omchak igneous complexes.

The Late Jurassic Baimka gabbro–diorite complex is represented by small stocks (0.1–0.5 km^2) and small dikes. The intrusions are composed of fine- to medium-grain gabbro, which is weakly propilitized as a rule.

The Early Cretaceous Egdykgych syenite–monzonite complex formed in an arc environment of Late Jurassic to Early Cretaceous age (Volkov et al., 2006). This complex comprises rocks of four intrusion phases: (1) porphyritic diorite, (2) monzodiorite, (3) syenite, and (4) porphyry monzodiorite and quartz porphyry monzodiorite. Poprhyry copper–molybdenum mineralization of the trend is spatially related to the four-phase stocks and large dikes. The U/Pb zircon age of the Egdykgych rocks is 139–143 Ma (Moll-Stalcup, 1995; Kotova et al., 2012; Baksheev et al., 2014).

The Late Cretaceous Omchak Complex consists of comparatively large bodies of quartz porphyry and porphyry granodiorite, as well as dikes of these rocks, which are weakly altered.

Late Cretaceous basalt and andesite dikes intruding Upper Jurassic and Lower Cretaceous sediments are the latest magmatic rocks. Basalt and andesite are occasionally and weakly altered.

The Vesenny (western) and Eastern NW- and near-meridional trending faults and the Baimka and Nakhodka diagonal faults, to which thick fault and shear zones, subvolcanic bodies, and hydrothermal stockworks, veins, and small breccia bodies are related, determine the general morphology and structural features of the Baimka trend. The highly fractured zones close to the Baimka and Nakhodka faults host porphyry stockworks. Intrusive and volcanic sedimentary rocks are altered potassic, propylitic, sericite, and argillic.

The Baimka trend comprises four porphyry Cu–Mo–Au fields (from north to south): Yuryakh, Peschanka, Nakhodka and Omchak (Fig. 1); the second and third are the most important and best studied.

We have studied precious metal mineralization at the Peschanka deposit, Nakhodka ore field, and the

Pravyi Svetlyi and Vilka occurrences in the Omchak ore field.

The Peschanka deposit is 22 km^2 in area; the indicated and inferred reserves and reserve development approved by the State Commission on Mineral Resource Reserves of the Russian Federation to January 1, 2012, at a 0.4% copper cutoff grade are as follows: 960.11 Mt of ore, 6.68 Mt of copper, 177.35 kt of molybdenum, 378.11 t of gold, and 3497 t of silver (Chitalin et al., 2013). The deposit is located in the eastern part of the large multiphase Egdykgych pluton intruding the Upper Jurassic volcanic sedimentary sequence. This pluton is composed of the predominant second-phase monzodiorite and minor third-phase syenite (Fig. 2a). The second-phase rock is intruded by fourth-phase porphyry monzodiorite and quartz monzodiorite, to which ore mineralization is spatially and paragenetically related.

Biotite–quartz–potassium feldspar rock (potassic alteration) cut by numerous quartz–sericite zones is the predominant type of alteration. Quartz–sericite zones ranging from 1 to 10 m in thickness form the megastockwork. Propylite is found in the outer part of the alteration halo. Postore argillic alteration is extremely rare at the deposit.

The orebodies are zones of stringer and impregnated ores and near-meridional trending quartz stockworks cutting quartz–sericite and potassic alterations. Ore minerals impregnate biotite–quartz–potassium feldspar and quartz–sericite alterations, are constituents of veins and veinlets, and are found in rare late-ore hydrothermal breccias with quartz–sulfide cement. Pyrite, chalcopyrite, and bornite are the major ore minerals. Molybdenite containing 1000–2000 ppm Re is less common.

Quartz–carbonate and fluorite veinlets, and postore near-horizontal gypsum–anhydrite veinlets are late hypogenic assemblages. The postore veinlets are concentrated within gently east-dipping (10–30°) sheetlike and lenticular stockworks up to a few meters thick. An en echelon near-horizontal system of veinlets within the stockworks (deformation zones) at oblique angles to their boundaries unambiguously indicates that these veinlets fill near-vertical extension and tensile fractures that resulted from thrusting in a simple strike-slip environment. The direction of extension within the veinlets is highlighted by near-vertical elongated gypsum crystals. Thrust zones are bounded neither by fault planes nor by sutural zones with milonites and cataclasites, indicating the early stage of thrusting, when only tensile fractures formed in the area of their dynamic action (extension of near-fault deformations). Some thrust zones host lenses of dry kakirite and fine-fragment tectonic breccias without any hydrothermal mineralization. According to exploration drilling, the thrust zones transect the deposit at various depths and crop out somewhere.

The Nakhodka ore field, 50 km^2 in area, comprises the Nakhodka, III Vesenny, Malysh, and Pryamoi porphyry copper–molybdenum prospects and the Vesenny Au–Ag deposit (Fig. 2b). Epithermal precious metal mineralization has been identified at the last three. The inferred resources of the ore field preliminarily estimated in 2012 by IMC Mount Consulting are as follows: 3.1 Mt of copper, 50 kt of molybdenum, 390 t of gold, and 2163 t of silver (Chitalin et al., 2013). The exploration of the ore field is ongoing.

The ore field comprises the Upper Jurassic tuffaceous terrigenous sediments intruded by the rocks of the Baimka and Egdykgych Complexes (Fig. 2b). Most part of the ore field is occupied by the porphyritic diorite intrusion that has been previously referred to the Late Jurassic to Early Cretaceous Vesenny Complex. However, the U/Pb zircon age of this rock is 142–143 Ma (Baksheev et al., 2014), which corresponds to that of the Egdykgych Complex. Crops-out of porphyry quartz monzodiorite, porphyritic diorite, and porphyry quartz diorite are comparatively small. According to Kotova et al. (2012), isotopic age of these rocks is 139.6 ± 0.5 Ma. Previously, Shavkunov (1973) and Shapovalov (1994) mentioned rocks of the Late Cretaceous Omchak Complex within the ore field. However, the U/Pb zircon data for the rocks referred to the Omchak Complex indicates that their age is consistent with that of the Egdykgych Complex (Kotova et al., 2012); therefore, they could be attributed to the latter.

The volcanic sedimentary sequence and intrusions are discordantly overlapped by sediments of the Early Cretaceous Ainakhkurgen Formation, which are retained only in the northeastern ore field.

The Late Cretaceous postore basalt and andesite dikes cutting all earlier intrusions, volcanic sedimentary and sedimentary sequences are the youngest within the ore field except for Quaternary alluvium.

Postore NW- and NE-trending strike slips and strike slip faults determine the ore field structure. Some of them inherit pre- and syn-mineralization faults.

Five alteration types are identified within the Nakhodka ore field (from early to late): (1) biotite–quartz–potassium feldspar, (2) propylitic (epidote–chlorite–actinolite, chlorite), (3) albite–chlorite–quartz–muscovite, (4) carbonate–tourmaline–albite–quartz–muscovite, and (5) quartz–illite.

The orebodies are isometric and slightly NW-extended zones of quartz and quartz–carbonate veilents hosted in quartz–sericite and quartz–illite alterations. Ores are related predominantly to quartz–sericite rocks; much less frequently ore minerals impregnate biotite–quartz–potassium feldspar alteration; the ores found in propylite are related to the narrow quartz–sericite zones. Pyrite, bornite, and chalcopyrite are the major ore minerals. Molybdenite containing 20–1450 ppm Re is developed predomi-

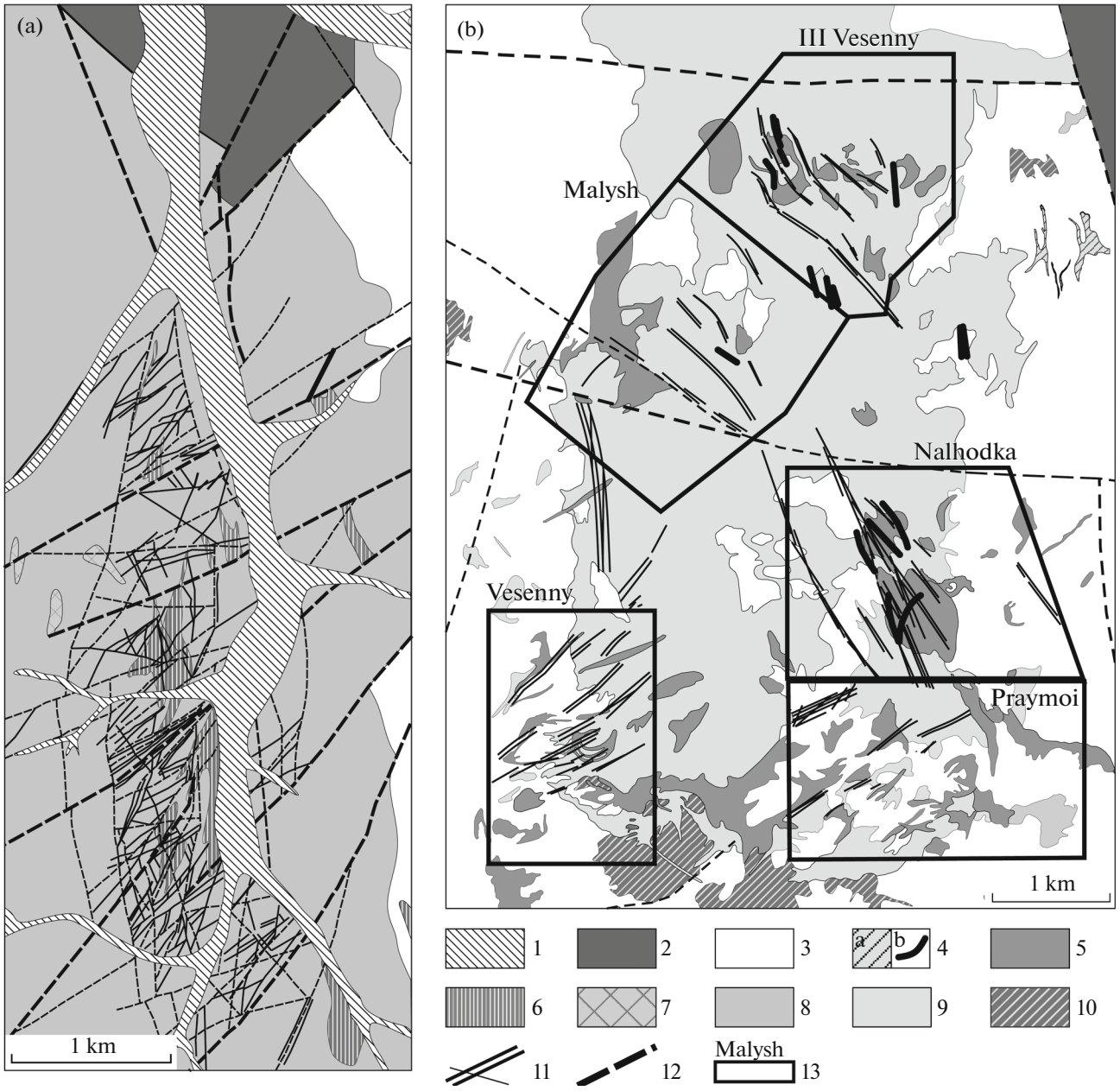

Fig. 2. Geological sketch maps of (a) Peschanka deposit and (b) Nakhodka ore field. (1) Quaternary sediments; (2) Lower Cretaceous sediments; (3) Upper Jurassic volcanic sedimentary rocks; (4) Late Cretaceous subvolcanic basalt: (a) stocks and sills, (b) dikes; (5–8) Early Cretaceous Egdykgych Complex: (5) porphyry quartz monzodiorite, porphyritic diorite, and porohyrytic quartz diorite, (6) porphyry monzodiorite and porphyry quartz monzodiorite, (7) syenite, (8) mozodiorite; (9) porphyritic diorite of Early Cretaceous Vesenny Complex; (10) Late Jurassic Baimka gabbro–diorite complex; (11) quartz–sericite alteration with ore-bearing quartz veinlets; (12) faults; (13) boundaries of prospects.

nantly at the Malysh prospect. Galena, sphalerite, and fahlores are abundant at the Vesenny deposit.

The Omchak ore field, 99 km^2 in area, comprising the Pravyi Svetlyi and Vilka prospects (not explored), is located at the northeastern flank of a gentle brachianticline composed of Upper Jurassic volcanic terrigenous rocks: andesite, basaltic andesite, tuff, tuffaceous conglomerate, tuffstone, conglomerate, siltstone and terrigenous sediments of the Ainakhkurgen Formation: conglomerate, gravelstone, and coarse-grained sandstone intercalated with siltstone.

The intrusive rocks are porphyritic diorite and monzodiorite of the Early Cretaceous Egdykgych Complex and porphyry granodiorite of the Late Cretaceous Omchak Complex. Porphyritic diorite is common predominantly in the northwestern and south-

eastern ore field. In the northeastern ore field, this rock composes isolated small bodies at the Vesenny Rise, which could be cropped-out fragments of the large pluton. In the southeastern ore field, a group of small porphyritic diorite bodies are located in the anticline with the Upper Jurassic volcanic sedimentary rocks in the core.

NW-, NE-, and near-meridional-trending faults are identified within the ore field. The NW-trending faults related to the Egdykgych deep-seated fault are the most important. The near-meridional faults belonging to the zone of the Aluchin deep-seated fault are common in the eastern part of the ore field. The NE-trending short faults are probable splays of Aluchin and Egdykgych deep-seated faults.

The following types of altered rock have been identified within the ore field: epidote–chlorite propylite, and quartz–sericite, calcite–chlorite–potassium feldspar–quartz–illite, and quartz–adularia–calcite–chlorite rocks.

The orebodies are veinlet zones with copper mineralization hosted in quartz–sericite alteration and propylite. In addition, zones of calcite–quartz veinlets with base-metal mineralization hosted in propylite and calcite–chlorite–potassium feldspar–illite rock were identified. Pyrite and chalcopyrite, and galena and sphalerite are the major ore minerals in the veinlet zones and calcite–quartz veinlets, respectively.

METHODS

A microscopic study was performed on an Axioplan Zeiss microscope equipped with a digital photo camera and computer at the Division of Mineralogy, Moscow State University.

The chemical composition of minerals was measured with a Jeol JSM-6480LV SEM equipped with an INCA-Energy 350 EDS with an Si–Li solid-state detector at the Laboratory of High Spatial Resolution Analytical Techniques, Division of Petrology, Moscow State University, analysts L.I. Marushchenko and V.O. Yapaskurt. The results were processed with the SEM Control User Interface v. 7.11 (Jeol Technics LTD) and INCA v. 17a (Oxford Instruments). The chemical composition was measured at an accelerating voltage of 20 kV, current intensity of 2 nA, and beam diameter of 1–3 μm. The detection limit and relative uncertainty of a single measurement range from 0.05 to 0.5 wt % depending on the concentration and excitation energy of spectral lines used in measurements. The absolute uncertainty of a single measurement does not exceed 1–2% for the major constituents and up to 10% for admixtures.

The following natural and synthetic sulfides and tellurides were used as reference materials: sphalerite (S, Zn), Mn metallic (Mn), chalcopyrite (Fe, Cu); arsenopyrite (As); alloy $Ag_{25}Au_{75}$ (Ag, Au), stibnite (Sb), PbTe (Te), PbSe (Se), Bi_2S_3 (Bi).

The chemical composition of native gold was determined with a Camebax SX-50 electron microprobe operating with an accelerating voltage of 15 kV, current intensity of 30 nA, and beam diameter of 1–3 μm at the Division of Mineralogy, Moscow State University, analyst I.A. Bryzgalov. The following standards were used: $AuTe_2$ (Au, Te), Cu (Cu), Ag_2Te (Ag). The detection limit is 0.02 wt %, the uncertainty of a single measurement does not exceed 2% for the major constituents and much higher for admixtures (about 10% relative). The PAP corrections are used for the correction procedure.

The chemical composition of a drilled core was measured at the certified laboratory Stewart Geochemical and Assay in Moscow. The following measurements were performed: (1) fire assay with the ICP-OES finish for Pt, Pd, and Au with a detection limit of 0.01 ppm, and (2) ICP-OES after oxidative dissolution of samples in an acid mixture for 40 chemical elements with the following detection limits for the major and accompanying elements, ppm: 0.5 Ag, 5 As, 5 Bi, 1 Cd, 1 Cu, 100 Fe, 1 Mn, 1 Mo, 2 Pb, 5 Sb, 10 Se, 10 Te, and 1 Zn. Samples containing more than 1% Cu were reanalyzed using a different sample preparation: oxidative dissolution with HBr followed by ICP-OES. The uncertainty of a single measurement is ±5%. Systematic and random uncertainty is within the range of $1.13 > \delta_{syst} > 0.84$ and $1.32 > \delta_{rand} > 1.0$, respectively.

In addition to the chemical data, the mineralogy of the drilled core with estimation of the sulfide grade in each sampling interval, documented by geologists of Sibgeoconsulting LLC, was used.

Fluid inclusions were studied in twice-polished plates of quartz, sphalerite and fluorite about 0.3–0.5 mm in thickness, first optically at room temperature, then with a Linkam THMSG-600 freezing/heating stage equipped with an Olympus BX51 optical microscope, videocamera, and computer at the Institute of Geology of Ore Deposits, Mineralogy, Geochemistry, and Petrography, Russian Academy of Sciences, Moscow, Russia. The chemical composition of fluid entrapped in inclusions was estimated from phase transitions and transformations during heating and freezing. The measurement uncertainty is ±0.2°C in the range of –20 to +20°C and decreases beyond this range. The composition of salts predominant in fluid inclusion solutions was estimated from the eutectic temperature (Borisenko, 1977). The salinity was estimated from final melting temperatures of ice according to experimental data on the $NaCl–H_2O$ system (Bodnar and Vityk, 1994). The CO_2 pressure was determined for immiscible fluids from the intersection of the isochore and isotherm (Kalyuzhny, 1982). The total pressure is the sum of partial pressures of CO_2 and saturated water vapor in the hydrothermal system (Prokofiev, 1998). Salinity, density and pressure of fluid were calculated with the FLINCOR program (Brown, 1989).

Bulk inclusion analysis of 0.5-g aliquots of milled quartz (0.25 to 0.5 mm sieved fraction) by gas chromatography, ion chromatography, and ICP-MS was carried out according to techniques reported by Kryazhev et al. (2006) at the Central Research Exploration Institute for Base and Precious Metals, Moscow, analyst Y.V. Vasyuta.

MINERALOGY OF PRECIOUS METAL ORES

Four types of precious metal-bearing ores were identified at the deposits and prospects of the Baimka trend: (I) porphyry chalcopyrite–bornite–quartz, (II) dolomite–quartz–polysulfide, (III) rhodochrosite–high-Mn dolomite-quartz–polysulfide, and (IV) quartz–calcite–polysulfide. Four types of assemblages with precious metal minerals correspond to them.

Type 1 is chalcopyrite + bornite + quartz assemblage with high-fineness native gold enclosed in bornite (prospect III Vesenny in the Nakhodka ore field) forming veinlets and impregnated in biotite–quartz–potassium feldspar and quartz–sericite alterations replacing monzonitic rocks of the Egdykgych Complex. The high gold grade was measured in bornite of the Peschanka deposit and the III Vesenny prospect. In most samples, Au minerals proper were not identified even by electron microscope. We suggest that in this case, gold occurs as tiny inclusions in bornite.

Type 2 is Mn-poor dolomite + quartz + sulfide (chalcopyrite, sphalerite, galena, tennantite-tetrahedrite) ± tourmaline assemblage with low-fineness gold and hessite (Peschanka deposit and Nakhodka, III Vesenny, and Pryamoi prospects in the Nakhodka ore field) filling veins and veinlets in quartz–sericite alteration and cutting veinlets with chalcopyrite and bornite.

Type 3 is rhodochrosite + high-Mn dolomite + quartz + sulfide (galena, sphalerite, chalcopyrite, tennantite-tetrahedrite) assemblage with low-fineness gold, electrum, Ag and Au–Ag tellurides, acanthite, and Ag sulfosalts filling veins and veinlets hosted in high-Mn dolomite–quartz–illite alteration (Vesenny deposit and Pryamoi prospect in the Nakhodka ore field). A comparatively high gold grade was measured at the Pryamoi prospect in the Nakhodka ore field within zones enriched in As-rich pyrite with other negligible sulfides. Arsenic-bearing pyrite containing up to 10.5 wt % As rims As-free pyrite. No Au species were found here; we suggest that gold occurs as tiny inclusions in As-rich pyrite.

Type 4 is a calcite + quartz + sulfide (chalcopyrite, sphalerite, galena) assemblage with low-fineness gold, Ag sulfides and selenides, and Ag-bearing sulfosalts. These minerals fill veinlets and impregnate potassium feldspar–calcite–chlorite–quartz and quartz–illite alterations at the Pravyi Svetlyi and Vilka prospects in the Omchak ore field and Malysh prospect in the Nakhodka ore field.

The morphological and compositional features of native gold and associated minerals were determined for each recorded assemblage.

In the type 1 assemblage, high-fineness *native gold* (917–926) was found as small inclusions (up to 10 μm) associated with clausthalite enclosed in bornite (Fig. 3a) at the III Vesenny prospect. In addition to bornite and chalcopyrite no any other sulfide minerals were found in this assemblage.

In the type 2 assemblage, optical microscopy revealed only native gold, whereas hessite was found in the course of detailed electron microscopic study.

Native gold and *hessite* occurs as grains ranging from a few to a few ten μm in size filling fractures in bornite and chalcopyrite. They are intimately intergrown with each other and clausthalite (Figs. 3b, 3c). The gold fineness, varying from 868 to 878, is lower than that of type 1 gold. Hessite occasionally contains Cu (1.3–1.6 wt %), which could have resulted from sulfide minerals trapped during electron microprobe analysis. However, S was not found. Therefore, we conclude that Cu is incorporated into the structure of the mineral.

In the type 3 assemblage, only native gold has been identified by optical microscope, whereas hessite, petzite, stützite, pearceite, and acanthite were found in an electron microscopic study. These minerals occur as fine inclusions (2–30 μm) or microveinlets in early sulfide minerals and are less frequently found within vein quartz and carbonates.

Native gold (fineness 756–857) and *electrum* (657–743) 2 to 30 μm in size are enclosed in pyrite, galena (Fig. 3d), and fahlores (Fig. 3e) and are intimately intergrown with hessite and petzite (Figs. 3b, 3h). Individual gold grains are weakly zoned: rims are enriched in Ag. A review of open file reports shows that the fineness of gold from placers (abandoned at present) within the Nakhodka ore field is consistent with that determined in primary ores. This suggests placer formation due to erosion of these ores.

Hessite, the most abundant Te mineral, is enclosed in earlier galena and chalcopyrite and is intimately intergrown with petzite, tennantite–tetrahedrite, and native gold (Fig. 3b). According to an electron microprobe study, hessite of the Vesenny deposit contains an admixture of Cu (up to 1.7 wt %), Fe (up to 0.4 wt %), As (up to 0.5 wt %) and Au (up to 0.6 wt %) (Table 1, an. 1–8). The absence of S in the composition suggests incorporation of Cu, Fe, and As into the mineral structure.

Petzite, stützite, pearceite, and acanthite are negligible in this assemblage.

Petzite. Electron microscopic study shows that hessite and petzite are intimately intergrown (Fig. 3h). Petzite contains admixture of Fe (up to 0.2 wt %) and

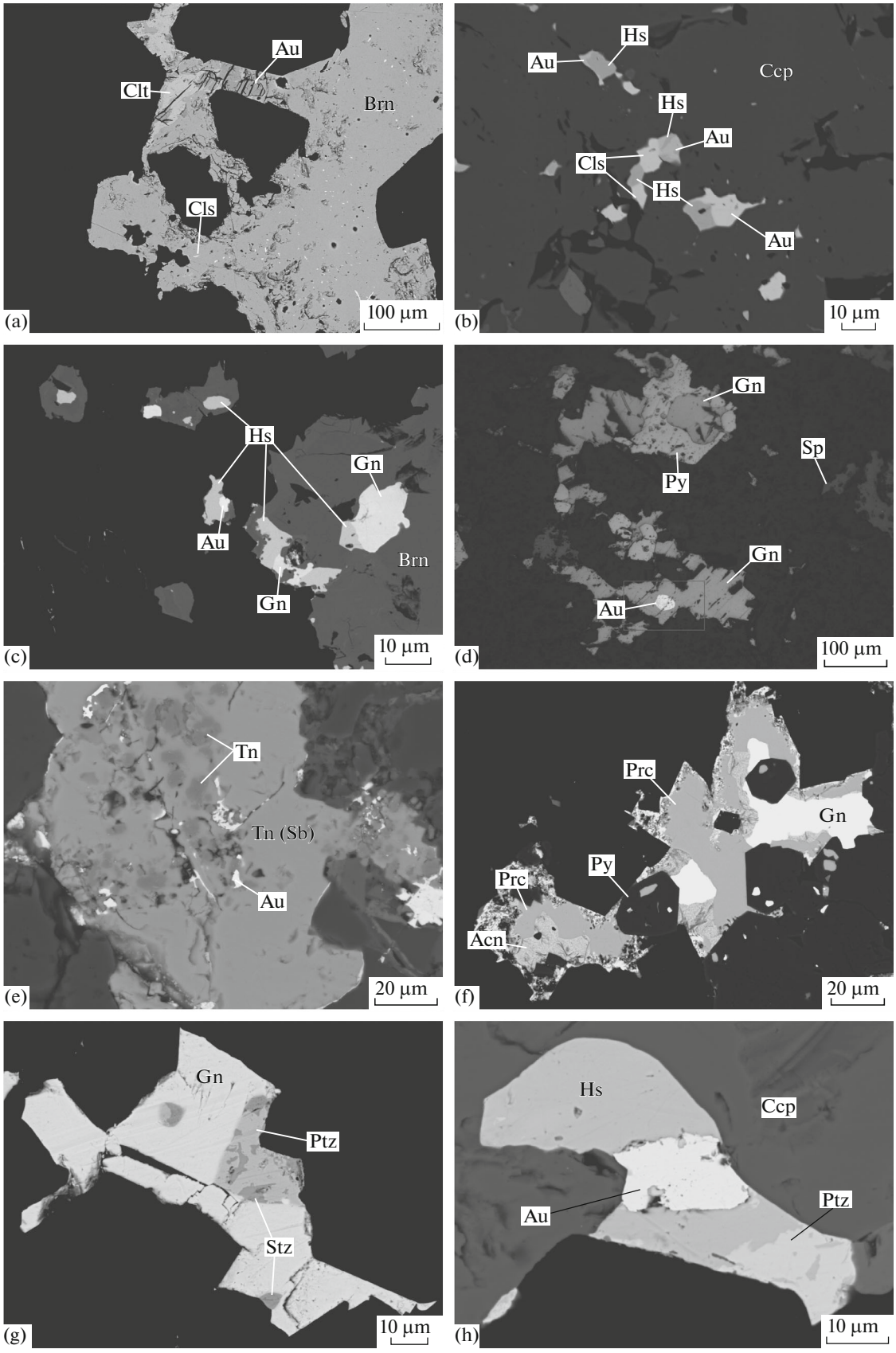
Au
Clt
Brn
Cls
100 μm
(a)
Hs
Au
Ccp
Hs
Au
Cls
Hs
Au
10 μm
(b)
Hs
Gn
Au
Brn
Gn
10 μm
(c)
Gn
Sp
Py
Gn
Au
100 μm
(d)
Tn
Tn (Sb)
Au
20 μm
(e)
Prc
Gn
Py
Prc
Acn
20 μm
(f)
Gn
Ptz
Stz
10 μm
(g)
Hs
Ccp
Au
Ptz
10 μm
(h)

Cu (up to 0.4 wt %) (Table 1, an. 9–11), which, similarly to hessite, are incorporated into the mineral structure rather than the constituents of sulfides trapped during electron microprobe analysis; this is consistent with the literature data on Fe and Cu incorporation into the mineral structure (Chvileva et al., 1988).

Stützite replaces earlier petzite (Fig. 3g). The largest mineral grains are 10 μm in size. Stützite contains up to 1.0 wt % Au (Table 1, an. 12), which most likely resulted from relics of replaced petzite.

Pearceite occurs as overgrowth rims up to 10 μm thick around galena (Fig. 3h), which is caused by the replacement of earlier tennantite, which frequently overgrows galena. Tennantite is replaced under the action of later Ag-bearing fluids. The mineral contains an admixture of Fe (up to 1.5 wt %, Sb (up to 1.3 wt %), and Te (up to 0.4 wt %) (Table 1, an. 13, 14).

Acanthite replaces pearceite (Fig. 3f), which is supported by Cu (2.6 wt %) (Table 1, an. 15).

The minerals of the type 4 assemblage are low-fineness gold, naumannite, Se-bearing pearceite, arsenopolybasite, acanthite, kurilite, and Pb–Ag–Bi–Te–Se, Ag–Te–Se, and Ag–Bi–Se phases.

Native gold occurs as fine inclusions (up to 10 μm) in chalcopyrite (Fig. 4a). Its fineness of 784–800 is close to that of native gold currently produced from a placer at Pravyi Svetlyi Creek.

Naumannite occurs as isolated inclusions up to 10 μm in size in chalcopyrite (Fig. 4b) and is intimately intergrown with pearceite enriched in Se (Fig. 4c). The mineral contains an admixture of Cu, Fe, S, and Te (Table 2, an. 1, 2). However, the first three elements could have been captured from the host chalcopyrite. The Te content ranges from 0.5 to 1.0 wt % (Table 2, an. 1, 2). This is the first finding of naumannite within the Baimka trend.

Se-rich pearceite occurs as grains up to a few tens of microns in size in quartz (Fig. 4d) and as intimate intergrowths with Se-bearing galena enclosed in chalcopyrite (Fig. 4e). The mineral contains Fe (up to 1.2 wt %), Sb (up to 2 wt %) and Te (up to 0.3 wt %) (Table 2, an. 3–7). Omchak pearceite differs drastically from pearceite at the Vesenny deposit in the Nakhodka ore field by a high concentration of Se ranging from 0.94 to 1.15 apfu.

Arsenopolybasite was identified in thin quartz veinlets cutting adularia–calcite–chlorite altered rock at the Pravyi Svetlyi prospect. The grain size is as large as a few tens of microns. The mineral contains Cu admixture (0.47–0.57 apfu) (Table 2, an. 8, 9).

Acanthite found at the Pravyi Svetlyi prospect occurs as fine (a few ten μm) grains in quartz and thin overgrowth rims on galena (Fig. 4f). In contrast to Cu-bearing acanthite from Vesenny in the Nakhodka ore field, this acanthite is free of admixtures. Its composition is as follows, wt %: 86.44 Ag, 10.37 S, total is 96.81; the empirical formula is $Ag_{2.137}S_{0.863}$.

Rare mineral *kurilite* was found only as a result of electron microprobe study. The chemical composition is as follows, wt %: 0.11 Pb, 67.58 Ag, 25.47 Te, 5.41 Se, 0.57 S, total is 99.15; the empirical formula calculated on the basis of 12 atoms is $Ag_{8.234}(Te_{2.624}Pb_{0.007})_{2.631}(Se_{0.900}S_{0.235})_{1.135}$. Kurilite was discovered at the Prasolovskoe Au–Ag deposit in Kurile in association with tetrahedrite, sylvanite, petzite, and hessite (Kovalenker et al., 2010).

The Pb–Ag–Bi–Te–Se, Ag–Te–Se, and Ag–Bi–Se phases associated with Se-rich galena and clausthalite are enclosed in chalcopyrite at the Malysh prospect (Fig. 4g). The very small size of inclusions (a few microns) hinders quantitative electron microprobe analysis of these phases.

FLUID INCLUSIONS

The examination of a great number of double-polished plates allowed us to find primary fluid inclusions more than 15 μm in size in quartz, fluorite, and sphalerite, which are applicable to the investigation. Twenty-two samples from veins and veinlets related to various mineral assemblages of the Baimka deposits and prospects were studied. Primary, pseudosecondary, and secondary fluid inclusions were distinguished using criteria of Roedder (1984). Primary inclusions are uniformly distributed within host mineral or occur parallel to growth zones. Secondary inclusions occur in trails abutting or crossing grain boundaries. Pseudosecondary inclusions heal the fractures within crystals, but these fractures do not reach the crystal surface; at the same time, the phase composition of these inclusions is similar to that of primary inclusions.

Three types of fluid inclusions were indentified in quartz (Fig. 5): (1) inclusions of chloride brines containing vapor bubbles, aqueous solution, one or several isotropic crystals, red lamellar hematite, and opaque minerals (chalcopyrite or magnetite), (2) vapor-rich inclusions containing vapor with a thin rim of an

Fig. 3. Precious metal mineralization of types 1–3. (a) First type, native gold enclosed in bornite; (b, c) second type: (b) intergrowth of native gold, clausthalite, and hessite, (c) intergrowth of galena, native gold and hessite; (d–g) third type: (d) native gold enclosed in galena, (e) native gold fills fracture in tennantite, (f) pearceite overgrows galena and is replaced by acanthite, (g) intergrowth of galena and petzite and replacement of the latter by stützite, (h) intergrowth of native gold, petzite, and hessite. (a, b) III Vesenny prospect, (c) Peschanka deposit, (d–h) Vesenny deposit. (a–c, e–h) Backscattered electron images, (d) photomicrograph in reflected light, normal light. (Au) Native gold, (Aan) acanthite, (Brn) bornite, (Ccp) chalcopyrite, (Cls) clausthalite, (Clt) chalcocite, (Gn) galena, (Hs) hessite, (Nm) naumannite, (Prc) pearceite, (Ptz) petzite, (Py) pyrite, (Sp) sphalerite, (Stz) stützite (Tn(Sb) and Tn) tennantite with the higher and lower Sb content, respectively.

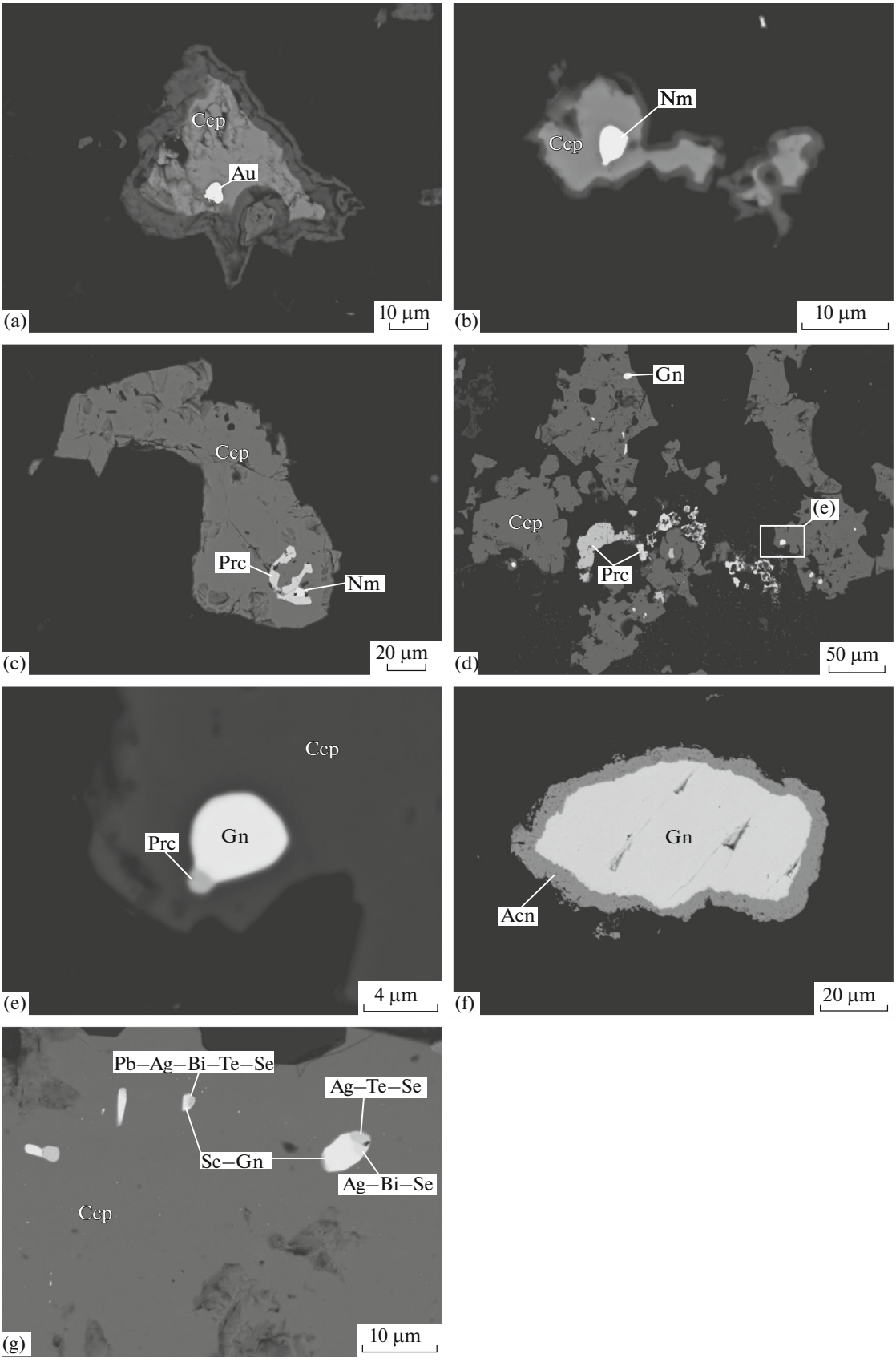
Ccp
Au
10 μm
(a)
Nm
Ccp
10 μm
(b)
Ccp
Prc
Nm
20 μm
(c)
Gn
Ccp
(e)
Prc
50 μm
(d)
Ccp
Prc
Gn
4 μm
(e)
Gn
Acn
20 μm
(f)
Pb–Ag–Bi–Te–Se
Ag–Te–Se
Se–Gn
Ag–Bi–Se
Ccp
10 μm
(g)

Table 1. Chemical composition (wt %) of Ag minerals, Nakhodka ore field

Component	1	2	3	4	5	6	7	8	9	10	11	12	13	14	15
Ag	63.05	63.67	60.69	63.58	63.03	62.63	62.10	60.04	43.18	42.11	42.40	58.69	66.61	63.26	81.84
Au	b.d.l.	b.d.l.	b.d.l.	b.d.l.	b.d.l.	b.d.l.	0.61	b.d.l.	24.16	24.07	24.82	1.01	b.d.l.	b.d.l.	b.d.l.
Te	36.51	36.31	37.49	36.14	35.92	36.64	37.10	40.16	32.06	32.19	32.46	41.22	b.d.l.	0.36	b.d.l.
As	b.d.l.	b.d.l.	b.d.l.	b.d.l.	0.53	b.d.l.	b.d.l.	b.d.l.	b.d.l.	b.d.l.	b.d.l.	b.d.l.	6.09	5.73	b.d.l.
Sb	b.d.l.	b.d.l.	b.d.l.	b.d.l.	b.d.l.	b.d.l.	b.d.l.	b.d.l.	b.d.l.	b.d.l.	b.d.l.	b.d.l.	1.16	1.34	b.d.l.
Fe	b.d.l.	b.d.l.	b.d.l.	0.35	b.d.l.	0.37	b.d.l.	b.d.l.	b.d.l.	0.20	b.d.l.	b.d.l.	0.21	1.47	b.d.l.
Cu	b.d.l.	b.d.l.	1.74	0.49	0.20	b.d.l.	b.d.l.	b.d.l.	b.d.l.	0.40	b.d.l.	b.d.l.	9.67	11.54	2.62
S	b.d.l.	b.d.l.	b.d.l.	b.d.l.	b.d.l.	b.d.l.	b.d.l.	b.d.l.	b.d.l.	b.d.l.	b.d.l.	b.d.l.	16.18	16.57	15.68
Total	99.57	99.98	99.91	100.57	99.67	99.64	99.80	100.20	99.41	98.97	99.68	100.92	99.93	100.26	100.13
Formula coefficients calculated on the basis of															
	3 atoms								6 atoms			8 atoms	29 atoms		3 atoms
Ag	2.014	2.024	1.910	1.994	2.001	1.992	1.986	1.916	3.102	3.023	3.049	4.990	13.080	12.137	1.766
Au							0.011		0.951	0.947	0.977	0.047			
Te	0.986	0.976	0.997	0.958	0.964	0.985	1.003	1.084	1.947	1.954	1.974	2.963		0.058	
As					0.024								1.722	1.582	
Sb													0.203	0.228	
Fe				0.021		0.023				0.028			0.081	0.543	
Cu			0.093	0.026	0.011					0.048			3.223	3.759	0.096
S													10.691	10.693	1.138

(1–2) Malysh prospect, (3–15) Vesenny deposit. (1–8) Hessite, (9–11) petzite, (12) stützite, (13, 14) pearceite, (15) acanthite. b.d.l. denotes that the element content is below detection limit.

aqueous solution, and (3) two-phase inclusions of aqueous solutions. Only type 3 inclusions were found in fluorite and sphalerite.

Microthermometric data on more than 400 single fluid inclusions from quartz, fluorite, and sphalerite from various deposits and prospects within the Baimka trend are summarized in Table 3 and Fig. 6.

The ore-forming fluids of the Baimka trend contained Na and K chlorides as indicated by the eutectic temperatures of inclusion solutions (–50 to –21°C). Daughter cubic halite crystals determined by the refraction index, similar to quartz and their transition into hydrohalite upon freezing of inclusion solutions (the reverse transition into halite occurs at 0.0–0.5°C), were established in multiphase inclusions. The fluid parameters of various ore types within the Baimka trend differ. High-temperature porphyry and medium- to low-temperature ores are distinguished.

Porphyry chalcopyrite–bornite–quartz ore was studied at the Peschanka deposit, and the III Vesenny, Malysh, and Pravyi Svetlyi prospects. The temperature and salinity ranges for fluids responsible for the formation of this ore are shown in Fig. 6a. All three inclusion types are found in quartz pertaining to this type.

The total homogenization of brine inclusions (type 1) in quartz (upon dissolution of all daughter phases) is gained at 594–301°C; the salinity is 73.1–32.2 wt % NaCl equiv. The fluid density is 0.97–1.36 g/cm^3. Vapor-rich fluid inclusions (type 2) syngenetic to high-temperature brine inclusions contain low-density water vapor and a small portion of aqueous fluid with a salinity ranging from 21.5 to 2.4 wt % NaCl equiv. They homogenize into vapor in the range of 594 to 381°C. CO_2 crystal appears upon deep freezing of some inclusions and dissolves at temperatures above –100°C. The saturated water pressure was 1200–220 bar.

Fig. 4. Backscattered electron images of minerals of type 4 precious metal mineralization. (a) Native gold enclosed in chalcopyrite, (b) naumannite enclosed in chalcopyrite, (c) aggregate of naumannite and Se-bearing pearceite enclosed in chalcopyrite, (d) isolated grain of Se-bearing pearceite, (e) intergrowth of Se-bearing galena and pearceite enclosed in chalcopyrite, magnified fragments of d, (f) overgrowth rim of acanthite on galena, (g) phases Pb–Ag–Bi–Te–Se, Ag–Te–Se, and Ag–Bi–Se intergrown with Se-bearing galena enclosed in chalcopyrite (a, f) Pravyi Svetlyi prospect, (b–e) Vilka prospect, (g) Malysh prospect. See Fig. 3 for mineral abbreviations.

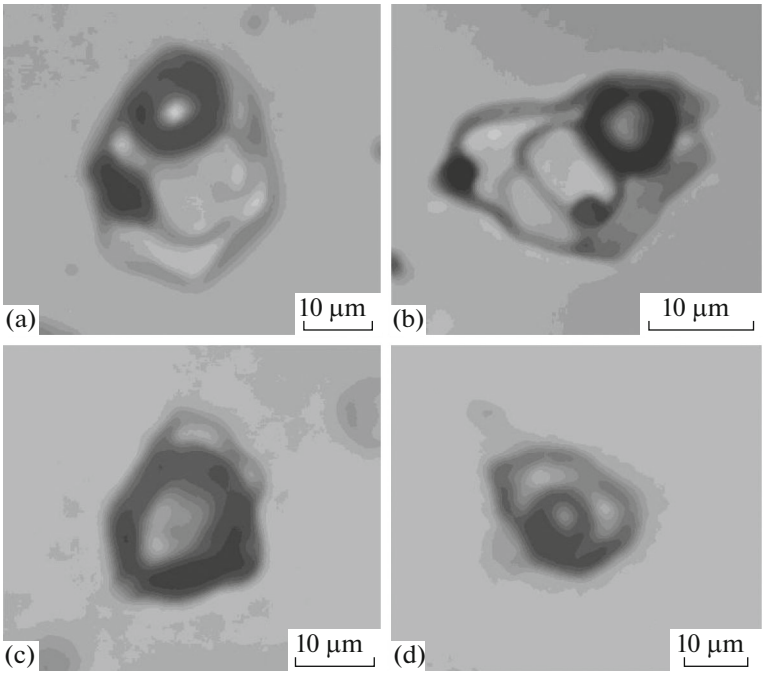

Fig. 5. Micrographs of fluid inclusions types from quartz of ore-bearing veinlets at deposits and prospects of Baimka trend. (a, b) Multiphase inclusions of high-temperature chloride brines containing aqueous solution, vapor bubble, cubic chloride crystals, and ore minerals (chalcopyrite (?), hematite), (c) vapor-rich inclusions, (d) two-phase inclusions of aqueous solution.

Table 2. Chemical composition (wt %) of Ag minerals, Omchak ore field

Comp.	1	2	3	4	5	6	7	8	9
Ag	73.88	75.71	58.02	58.21	62.20	61.70	62.30	74.94	76.42
Cu	2.24	1.27	14.62	13.87	11.68	12.24	11.72	1.28	1.61
Fe	0.57	0.93	1.06	0.63	b.d.l.	1.16	b.d.l.	b.d.l.	b.d.l.
As	b.d.l.	b.d.l.	5.86	5.70	6.16	5.09	6.17	3.26	4.31
Sb	b.d.l.	b.d.l.	1.56	1.99	b.d.l.	b.d.l.	b.d.l.	3.96	3.61
Te	0.52	0.97	b.d.l.	b.d.l.	b.d.l.	b.d.l.	0.27	b.d.l.	b.d.l.
S	3.36	4.85	14.59	14.62	14.66	14.41	14.55	14.66	15.23
Se	18.60	14.77	4.34	4.60	3.58	4.22	3.44	b.d.l.	b.d.l.
Total	99.17	98.50	100.05	99.62	98.28	98.82	98.45	98.10	101.18
Formula coefficients calculated on the basis of									
	3 atoms		29 atoms						
Ag	1.912	1.942	11.238	11.373	12.431	12.230	12.464	16.142	15.853
Cu	0.098	0.055	4.805	4.601	3.964	4.119	3.981	0.467	0.568
Fe	0.028	0.046	0.397	0.237		0.443			
As			1.634	1.604	1.773	1.454	1.776	1.012	1.287
Sb			0.268	0.345					
Te	0.011	0.021					0.045		
S	0.293	0.418	9.510	9.613	9.856	9.610	9.794	10.623	10.629
Se	0.657	0.517	1.147	1.227	0.976	1.144	0.939		

(1–7) Vilka prospect, (8, 9) Pravyi Svetlyi prospect. (1, 2) Naumannite, (3–7) Se-bearing pearceite, (8, 9) arsenopolybasite. b.d.l. denotes that the element content is below detection limit.

Table 3. Microthermometric data for individual fluid inclusions from minerals of various type ores at deposits and prospects of Baimka trend

Number of sample	Type of inclusion	*n*	T_{hom}, °C	T_{eut}, °C	$T_{ice\ melt}$, °C	$T_{CO_2\ melt}$, °C	Salinity wt % NaCl equiv	*d*, g/cm^3	*P*, bar
Porphyry chalcopyrite–bornite–quartz ore									
Peschanka (quartz)									
SP 10 282/35.6	1, P	4	506	n.d.	(442)	–	52.3	1.11	–
	1, P	6	414	n.d.	(497)	–	49.0	1.09	–
	1, P	3	436	n.d.	(485)	–	51.6	1.10	–
	1, P	5	226	n.d.	(464)	–	55.0	1.36	–
	1, P	3	364	n.d.	(454)	–	53.8	1.21	–
	1, P	8	256	n.d.	(448)	–	53.0	1.29	–
	2, P	4	447 G	n.d.	–5.0	–	7.9	n.d.	420
	2, P	7	439 G	n.d.	–1.4	–100 Sbl	2.4	n.d.	390
	2, P	6	430 G	n.d.	–3.8	–	6.2	n.d.	360
	2, P	3	424 G	n.d.	–3.4	–	5.5	n.d.	340
	2, P	3	406 G	n.d.	–2.1	–	3.5	n.d.	290
	1, P	5	439	n.d.	(411)	–	48.7	1.09	–
	1, P	5	255	n.d.	(405)	–	48.0	1,24	–
	1, P	11	267	n.d.	(374)	–	44.7	1,19	–
	3, PS	4	280	–22	–4.7	–	7.5	0.83	–
	3, S	3	117	–21	–1.8	–	3.1	0.97	–
DHP13–297/795.3	1, P	2	349	–55	(469)	–	55.7	1.25	–
	1, P	5	304	–55	(425)	–	50.3	1.22	–
	1, P	3	273	–55	(387)	–	46.1	1.20	–
	1, PS	3	311	–56	(365)	–	43.8	1.14	–
	1, PS	8	313	–56	(206)	–	32.2	1.02	–
	2, P	3	479 G	–40	–18.7	–	21.5	n.d.	540
	2, P	2	435 G	–51	–8.8	–	12.6	n.d.	370
	2, PS	2	381G	–33	–3.7	–	5.9	n.d.	220
	3, P	3	367	–37	–6.2	–	9.5	0.71	–
	3, P	2	348	–31	–4.6	–	7.3	0.71	–
	3, PS	2	316	–30	–2.5	–	4.1	0.72	–
	3, S	3	113	–33	–0.6	–	1.0	0.96	–
III Vesenny (quartz)									
7732–8122	3, P	3	330	–26	–0.6	–	1.1	0.63	–
	3, PS	3	257	–24	–0.5	–	0.9	0.79	–
	3, S	2	119	–24	–0.5	–	0.9	0.95	–

Table 3. (Contd.)

Number of sample	Type of inclusion	*n*	T_{hom}, °C	T_{eut}, °C	$T_{ice\ melt}$, °C	$T_{CO_2\ melt}$, °C	Salinity wt % NaCl equiv	*d*, g/cm^3	*P*, bar
Malysh (quartz)									
7985–5050	1, P	2	545	–38	(362)	–	43.5	1.08	–
	1, P	3	305	n.d.	(396)	–	47.0	1.09	–
	3, P	2	318	–30	–6.1	–	9.3	0.79	–
7623–038	3, 2, P	3	460	–55	–14.7	–	18.4	0.69	470
	3, 2, P	4	401	–57	–11.8	–	15.8	0.75	270
	3, PS	6	375	–28	–1.6	–	2.6	0.55	–
	3, P–B	3	290	–28	–1.6	–	2.6	0.75	–
Pravyi Svetlyi (quartz)									
6620–8701/1	1, 2, P	3	558	–50	(594)	–	73.1	1.35	1200
	1, 2, P	4	488	–53	(376)	–	44.9	0.97	580
	1, PS	3	59	–55	(301)	–	38.2	1.26	–
	3, S	3	159	–28	–2.7	–	4.4	0.94	–
	3, S	4	145	–29	–2.1	–	3.4	0.95	–
	3, S	5	139	–28	–7.3	–	10.9	1.01	–
	3, S	3	106	–31	–2.5	–	4.1	0.98	–
Dolomite–quartz–polysulfide ore									
Peschanka (quartz)									
8295–757	3, P	2	293	–32	–4.2	–	6.7	0.80	–
	3, P	2	292	–28	–0.9	–	1.6	0.73	–
	3, P	2	288	–30	–0.7	–	1.2	0.73	–
	3, P–B	4	265	–28	–0.2	–	0.4	0.77	–
	3, P–B	2	215	–29	–0.4	–	0.7	0.85	–
	3, P–B	3	160	–29	–0.2	–	0.4	0.92	–
Peschanka (fluorite)									
SP10 230–65.6	3, P	2	265	–30	–0.1	–	0.2	0.76	–
	3, P	4	244	–32	–0.6	–	1.1	0.78	–
	3, P	9	198	–31	–0.5	–	0.9	0.88	–
	3, S	3	159	–24	–0.2	–	0.4	0.92	–
	3, S	2	129	–34	–1.8	–	3.1	0.96	–
	3, S	3	128	–22	–0.2	–	0.4	0.94	–
	3, S	2	104	–21	–0.2	–	0.4	0.96	–
Nakhodka (quartz)									
SN11 540–542.5	1, P	4	581	n.d.	(452)	–	53.5	0.99	–
	2, P	2	540 G	–23	–5.9	–	9.1	n.d.	850
	1, P	3	362	–47	(485)	–	57.8	1.14	–
	1, P	2	298	–50	(485)	–	57.8	1.14	–
	2, P	2	460 G	–25	–7.2	–	10.7	n.d.	470
	1, P	2	309	–48	(430)	–	50.8	1.10	–
	2, P	3	402 G	–23	–2.8	–	4.7	n.d.	280

Table 3. (Contd.)

Number of sample	Type of inclusion	*n*	T_{hom}, °C	T_{eut}, °C	$T_{ice\ melt}$, °C	$T_{CO_2\ melt}$, °C	Salinity wt % NaCl equiv	*d*, g/cm^3	*P*, bar
	3, P	2	346	–21	–1.2	–	2.1	0.61	–
	3, PS	3	264	–25	–1.5	–	2.6	0.80	–
	3, S	3	130	–26	–3.1	–	5.1	0.97	–
	3, S	3	122	–26	–2.9	–	4.8	0.98	–
Praymoi (quartz)									
7231–8125–2	1, P	2	250	–55	(418)	–	49.5	1.10	–
	3, P	3	362	–37	–2.4	–	4.0	0.61	–
	3, PS	3	261	–32	–6.5	–	9.9	0.88	–
7246–8266	3, P	3	418	–36	–7.5	–	11.1	0.63	–
	3, P	2	391	–46	–16.3	–	19.7	0.82	–
	1, P	4	202	n.d.	(315)	–	39.4	1.09	–
	3, PS	7	285	–31	–2.4	–	4.0	0.78	–
	3, PS	3	253	–28	–0.6	–	1.1	0.80	–
	3, S	2	233	–26	–0.5	–	0.9	0.83	–
	3, S	6	158	–26	–0.4	–	0.7	0.92	–
Rhodochrosite–high–Mn dolomite–quartz–polysulfide ore									
Vesenny (quartz)									
7303–8000–2	3, 2, P	3	404	–58	–23.8	–	22.9	0.83	280
	3, 2, P	2	402	–37	–10.8	–	14.8	0.73	280
	3, P	3	380	–55	–7.3	–	10.9	0.70	–
	3, PS	5	259	–32	–2.3	–	3.8	0.82	–
Vesenny (sphalerite)									
SN11–721–138.6	3, P	12	168	–31	–2.6	–	4.3	0.93	–
SN11–721–364.5	3, P	6	275	–32	–3.9	–	6.3	0.82	–
	3, P	2	214	–34	–1.7	–	2.9	0.87	–
	3, P	7	211	–34	–2.1	–	3.6	0.88	–
	3, P	5	203	–29	–0.7	–	1.2	0.87	–
	3, P	19	197	–34	–2.5	–	4.2	0.90	–
	3, P	2	156	–24	–2.5	–	4.2	0.94	–
Pryamoi (quartz)									
7240–818	2, P	2	395 G	–24	–1.6	–	2.7	n.d.	260
	3, P	2	309	–31	–4.1	–	6.6	0.77	–
	1, P	3	298	–37	(289)	–	37.4	1.08	–
	3, P	2	296	–33	–5.4	–	8.4	0.82	–
	3, P	3	270	–21	–2.5	–	4.2	0.81	–
	3, PS	2	257	–35	–6.6	–	10.0	0.89	–
Quartz–calcite–polysulfide ore									
Pravyi Svetlyi (quartz)									
6894–8724	2, P	2	400 G	–27	–5.1	–	8.0	n.d.	270
	3, P	3	389	–35	–3.5	–	5.6	0.57	–

Table 3. (Contd.)

Number of sample	Type of inclusion	*n*	T_{hom}, °C	T_{eut}, °C	$T_{ice\ melt}$, °C	$T_{CO_2\ melt}$, °C	Salinity wt % NaCl equiv	*d*, g/cm^3	*P*, bar
	3, P	3	383	–23	–0.9	–	1.5	0.49	–
	3, P	3	307	–30	–6.1	–	9.3	0.81	–
	3, P	5	301	–34	–3.6	–	5.8	0.77	–
	1, P	3	296	–59	(284)	–	37.0	1.09	–
	3, S	4	130	–33	–2.9	–	4.7	0.97	–
	3, S	2	128	–44	–13.3	–	17.2	1.06	–
Vilka (quartz)									
7065–9149	3, 2 P	3	362	–29	–0.3	–	0.5	0.53	180
	3, 2 P	7	356	–28	–0.3	–	0.5	0.55	170
	3, PS	4	277	–27	–0.4	–	0.7	0.75	–
	3, S	5	179	–27	–0.3	–	0.5	0.90	–
	3, B	9	162	–28	–0.2	–	0.3	0.91	–
7127–8361	3, P	4	230	–24	–1.7	–	2.8	0.85	–
	1, P	8	204	–24	–1.7	–	2.8	0.88	–
	3, PS	10	171	–25	–1.8	–	3.0	0.92	–
Malysh (quartz)									
7583–951	3, P	3	342	–32	–0.8	–	1.4	0.61	–
	3, P	2	319	–38	–1.6	–	2.7	0.69	–
7960–5350	3, P	2	303	–27	–0.4	–	0.7	0.69	–
	3, P	3	278	–28	–1.3	–	2.2	0.77	–
	3, P	2	273	–25	–2.2	–	3.7	0.79	–
	3, P	6	270	–33	–0.4	–	0.7	0.76	–
	3, S	2	139	–27	–1.6	–	2.7	0.95	–
7975–5750	3, P	2	331	–27	–2.7	–	4.5	0.69	–
	3, P	3	274	–25	–2.4	–	4.0	0.80	–
	3, PS	2	255	–24	–1.8	–	3.1	0.82	–
	3, S	3	226	–23	–6.1	–	9.3	0.91	–
	3, S	2	166	–24	–1.4	–	2.4	0.92	–
	3, S	3	162	–26	–2.2	–	3.7	0.94	–
	3, S	3	129	–27	–0.5	–	0.9	0.95	–
7583–951	3, P	3	342	–32	–0.8	–	1.4	0.61	–
	3, P	2	319	–38	–1.6	–	2.7	0.69	–
7960–5350	3, P	2	303	–27	–0.4	–	0.7	0.69	–
	3, P	3	278	–28	–1.3	–	2.2	0.77	–
	3, P	2	273	–25	–2.2	–	3.7	0.79	–
	3, P	6	270	–33	–0.4	–	0.7	0.76	–
	3, S	2	139	–27	–1.6	–	2.7	0.95	–
7975–5750	3, P	2	331	–27	–2.7	–	4.5	0.69	–
	3, P	3	274	–25	–2.4	–	4.0	0.80	–
	3, PS	2	255	–24	–1.8	–	3.1	0.82	–
	3, S	3	226	–23	–6.1	–	9.3	0.91	–
	3, S	2	166	–24	–1.4	–	2.4	0.92	–
	3, S	3	162	–26	–2.2	–	3.7	0.94	–
	3, S	3	129	–27	–0.5	–	0.9	0.95	–

(P) Primary inclusions, (PS) pseudosecondary inclusions, (S) secondary inclusions. Types of inclusions: (1) brine inclusions, (2) vapor-rich, (3) aqueous solutions. (G) Homogenization into vapor, (Sbl) sublimation of CO_2. n.d. denotes that this parameter was not determined.

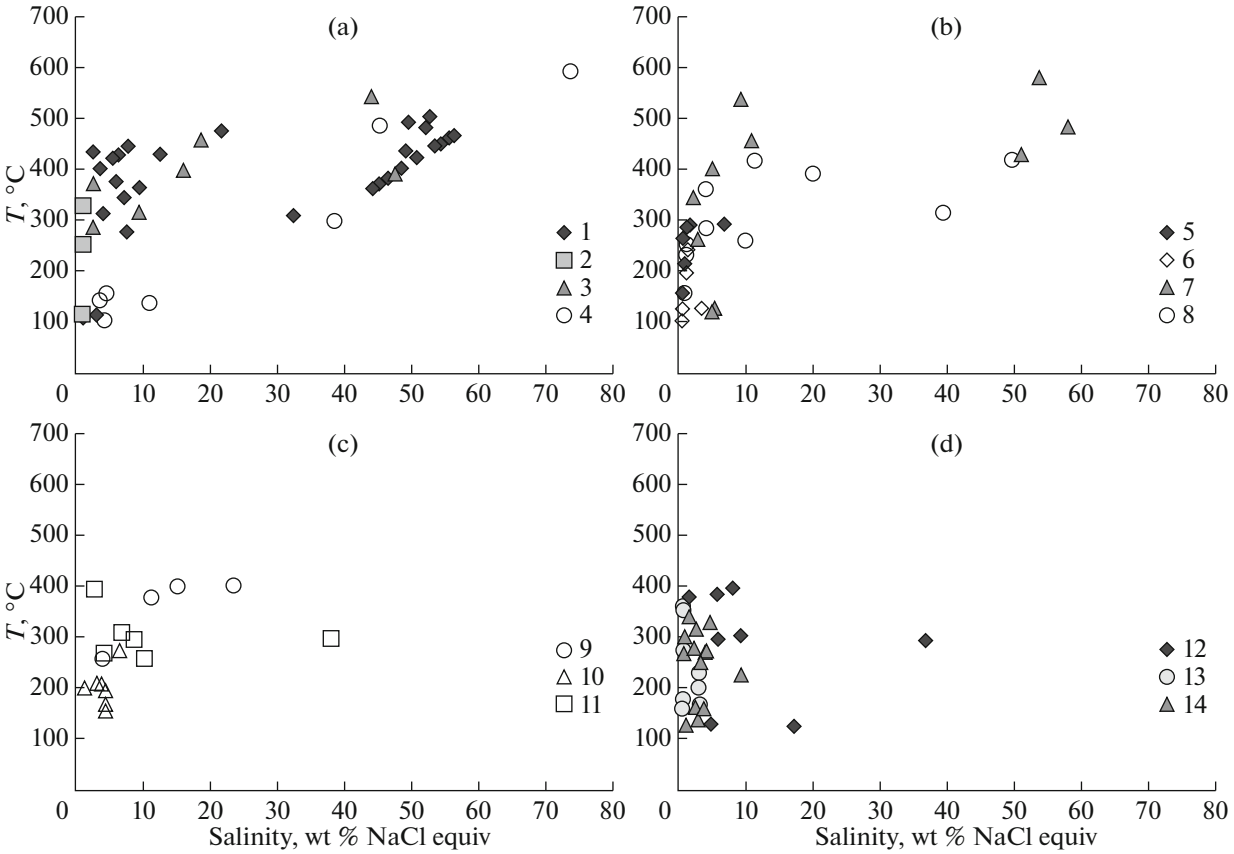

Fig. 6. Temperature versus salinity diagrams for ore-forming fluids of various assemblages within Baimka trend. (a) Porphyry chalcopyrite–bornite–quartz ((1) Peschanka, quartz, (2) Vesenny, quartz, (3) Malysh, quartz, (4) Pravyi Svetlyi, quartz); (b) dolomite–quartz–polysulfide ((5) Peschanka, quartz, (6) Peschanka, fluorite, (7) Nakhodka, quartz, (8) Pryamoi, quartz); (c) rhodochrosite–high-Mn dolomite–quartz–polysulfide ((9) Vesenny, quartz, (10) Vesenny, sphalerite, (11) Pryamoi, quartz); (d) quartz–calcite–polysulfide ((12) Pravyi Svetlyi, quartz, (13) Vilka, quartz, (14) Malysh, quartz).

The two-phase (type 3) fluid inclusions in quartz homogenize into liquid at 460–106°C; the salinity is 18.4–0.9 wt % NaCl equiv; the fluid density ranges from 0.63 to 1.01 g/cm^3.

The composition of inclusion solutions in porphyry-stage quartz at the Peschanka deposit and Malysh prospect is given in Table 4 and Fig. 7a.

In the fluids, the major cations are Na and K, while Ca and Mg are the minor cations. Appreciable contents of Cl^-, HCO_3^-, CO_2, CH_4, As, and B were measured. In addition, the following microcomponents were measured: Br, Li, Rb, Cs, Sr, Mo, Sb, Zn, Cd, Bi, Ga, Ge, Sc, Mn, Fe, Co, Ni, Cr, Sn, Ba, W, Hg, Tl, and REE. The K/Rb value ranges from 186 to 284.

The dolomite–quartz–polysulfide ore was studied at the Peschanka deposit and the Nakhodka and Pryamoi prospects. The temperature and salinity ranges for fluids responsible for the formation of this ore are shown in Fig. 6b. All three inclusion types are found in quartz referred to this type.

The brine inclusions (type 1) in quartz homogenize at 581–315°C; salinity ranges from 53.5 to 39.4 wt % NaCl equiv. The fluid density is 0.99–1.14 g/cm^3. Vapor-rich fluid inclusions (type 2) syngenetic to the high-temperature brine inclusions and two-phase inclusions (type 3) contain low-density water vapor and small portion of aqueous fluid with salinity ranging from 10.7 to 4.7 wt % NaCl equiv. They homogenize into vapor in the range of 540 to 402°C. The saturated water pressure was 850–280 bar. The two-phase (type 3) fluid inclusions in quartz homogenize into liquid at 418–104°C; salinity is 11.1–0.2 wt % NaCl equiv; the fluid density ranges from 0.61 to 0.97 g/cm^3.

Study of the fluid composition (Table 4, Fig. 7b) revealed that the major cations are Na and K, while the minor ones are Ca and Mg. Appreciable contents of Cl^-, HCO_3^-, CO_2, CH_4, As (2.8 g/L, which is the highest concentration of this element in fluids within the Baimka trend), and B were measured. In addition to the microcomponents measured in the porphyry-stage fluid (Br, Li, Rb, Cs, Sr, Mo, Sb, Zn, Cd, Bi, Ga, Ge, Sc, Mn, Fe, Co, Ni, Cr, Sn, Ba, W, Hg, Tl, and REE), Ag, Pb, Th, Ti, V, and Zr were detected. The K/Rb value ranges from 426 to 2405.

Fluid inclusions in minerals of rhodochrosite–high-Mn dolomite–quartz–polysulfide ore were studied at the Vesenny deposit and Pryamoi prospect. The temperature and salinity ranges for fluids responsible for the formation of this ore are shown in Fig. 6c. Type 3 fluid inclusions are predominant in quartz and sphalerite. Occasional type 2 inclusions syngenetic to type 3 inclusions indicate an immiscible hydrothermal fluid. A group of brine inclusions was found in quartz from the Pryamoi prospect.

The type 1 brine inclusions in quartz homogenize at 298°C; the salinity is 37.4 wt % NaCl equiv. The fluid density is 1.08 g/cm^3. The two-phase (type 3) fluid inclusions in quartz homogenize into liquid at 404–257°C; salinity is 22.9–3.8 wt % NaCl equiv; the fluid density ranges from 0.70 to 1.08 g/cm^3. Vapor-rich fluid inclusions (type 2) syngenetic to the highest-temperature type 3 inclusions contain low-density water vapor and a small portion of aqueous fluid. They homogenize into vapor at 404–395°C; the pressure of water saturated vapor ranges from 280 to 260 bar.

Two-phase fluid inclusions of type 3 from sphalerite homogenize into liquid at 275–156°C; the salinity and fluid density ranges from 6.3 to 1.2 wt % NaCl equiv and from 0.82 to 0.94 g/cm^3, respectively.

Fluid inclusions from minerals of the quartz–calcite–polysulfide ore were examined at the Pravyi Svetlyi, Vilka, and Malysh prospects. The temperature and salinity ranges for fluids responsible for the formation of this ore are shown in Fig. 6d. The type 3 fluid inclusions are predominant in quartz. Occasional type 2 inclusions syngenetic to the type 3 inclusions indicate immiscible hydrothermal fluid. A group of brine inclusions was found in quartz from the Pravyi Svetlyi prospect.

The brine inclusions of type 1 in quartz homogenize at 296°C; salinity is 37.0 wt % NaCl equiv. The fluid density is 1.09 g/cm^3. Two-phase (type 3) fluid inclusions in quartz homogenize into liquid at 389–128°C; the salinity is 17.2–0.3 wt % NaCl equiv; the fluid density ranges from 0.53 to 1.06 g/cm^3. Vapor-rich fluid inclusions (type 2) syngenetic to the highest-temperature type 3 inclusions contain low-density water vapor and a small portion of aqueous fluid. They homogenize into vapor at 400–356°C; the pressure of water saturated vapor ranges from 270 to 170 bar.

The fluid inclusion study revealed that ores in the Baimka trend precipitated within a wide range of temperatures (594–104°C) and pressures (1200–170 bar) from hydrothermal fluid with strongly variable salinity. The certain range of physicochemical parameters and chemical composition of ore-forming fluid corresponds to each ore type.

Table 4. Bulk composition of fluid inclusions from quartz of various assemblages of some deposits and prospects in Baimka trend

Ore type	1		2	
Component	Peschanka	Malysh	Nakhodka	Pryamoi
Macrocomponents, g/kg of water				
CO_2	16.5	4.2	9.2	16.0
CH_4	0.19	0.01	0.14	0.07
Cl^-	50.3	9.9	10.1	9.90
HCO_3^-	269.2	53.0	54.8	85.2
Na	76.7	23.8	27.0	34.3
K	8.0	2.0	2.8	5.2
Ca	0.13	0.60	–	0.38
Mg	27.65	0.46	–	0.45
Microcomponents, 10^{-3} g/kg of water				
Br	673.6	316.7	44.1	25.9
As	1632	33.4	1805	2816
Li	0.76	1.58	2.61	7.50
B	903	331	1360	880
Rb	42.87	6.97	1.16	12.31
Cs	2.08	0.93	–	0.51
Sr	86.2	38.98	–	24.55
Mo	5.15	1.78	1.02	1.02
Ag	–	–	–	0.016
Sb	97.4	4.81	40.2	59.1
Zn	79.4	57.6	–	–
Cd	–	0.48	0.02	0.14
Pb	–	–	–	0.43
Bi	0.05	–	–	0.03
Th	–	–	–	0.02
Ga	51.7	–	–	–
Ge	0.93	0.15	0.28	0.75
Sc	1.27	–	–	1.02
Ti	–	–	–	0.86
Mn	730	101.3	–	72.4
Fe	195	–	–	15.46
Co	0.79	0.16	–	0.21
Ni	6.74	0.31	–	0.76
V	–	–	–	13.55
Cr	0.90	–	–	0.06
Zr	–	–	–	0.01
Sn	0.09	–	–	0.24
Ba	12.39	4.29	–	–
W	2.08	–	0.10	0.10
Hg	0.35	–	–	–
Tl	0.05	0.07	0.02	0.14
REE	0.19	–	–	0.08
La	0.07	–	–	0.02
Ce	–	–	–	0.04
Pr	–	–	–	0.02
Nd	–	–	–	0.01
K/Rb	186	284	2405	426

(1) Porphyry chalcopyrite–bornite–quartz ore, (2) dolomite–quartz–polysulfide ore. Dash denotes that component content is below detection limit.

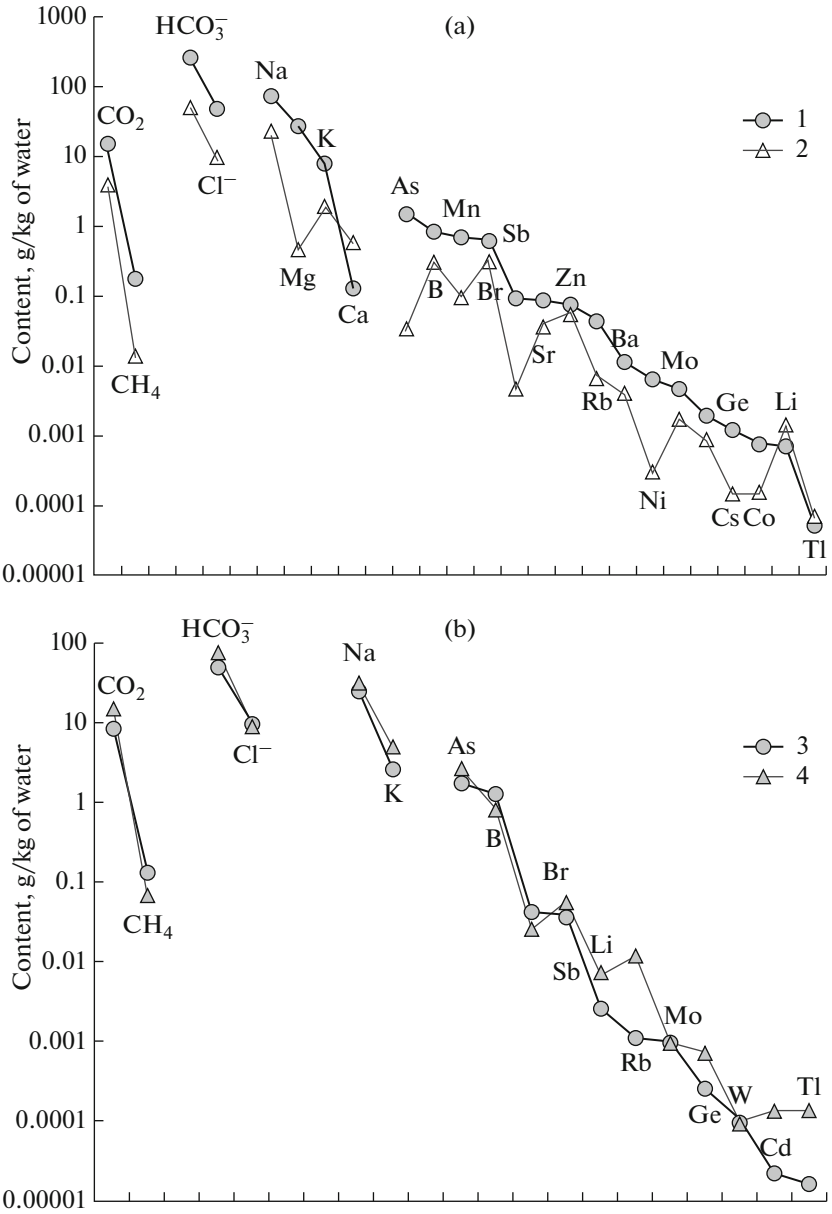

Fig. 7. Chemical composition of ore-forming fluid of (a) porphyry chalcopyrite–bornite–quartz and (b) dolomite–quartz–polysulfide assemblages. Deposits and prospects: (1) Peschanka, (2) Malysh, (3) Nakodka, (4) Pryamoi.

GEOCHEMICAL ZONING OF ORE-FORMING SYSTEMS

The study of geochemical zoning of the Peschanka and Nakhodka porphyry–epithermal systems (PES) is based on the chemical compositions of drilled cores obtained from the described area down to a depth of 300 m on average in 2010–2013. The geochemical data on drilled cores were processed by principal component analyses using Statistica software (Borovikov, 2013). As a result, we obtained six factors with a total contribution of 77% from the general variability of the anomaly geochemical field, which reflect the correlations between 14 ore elements (Table 5).

In accordance with their "weight," the elements are grouped into factors, or geochemical associations, which can be compared with the mineral assemblages of the major ore stages. A correlation between geochemical associations and ore stages is supported by the Pearson coefficient between the factor values and the content of the major ore minerals in the corresponding core intervals (Tables 6, 7).

The porphyry-stage ores of PES (type I ores) are characterized by factors 4–6. F4 scores correlate with the amount of pyrite that makes it possible to relate the Fe(MnAu) geochemical association to the earliest porphyry-stage gold–pyrite ore. F6 scores corre-

sponding to the Mo(Cu) association statistically correlate with the amount of chalcopyrite and molybdenite, which form the major mineral assemblage of porphyry Cu–Mo (chalcopyrite–molybdenite) ore. F5 scores correlate with the amount of bornite and chalcopyrite, which makes it possible to attribute the CuBi(Se) geochemical association to the highest grade bornite ore of the late porphyry stage.

The SbAs(CuSe) geochemical association correlated with the fahlore mineralization formed at the boundary between the porphyry and epithermal stages of the PES is interpreted unambiguously by F2 scores.

The epithermal ores (2–4 ore types) of the PES are characterized by the ZnPbCdMnAg(Au) and TeAuSe(Ag) associations, which are distinguished by factors 1 and 3. According to the composition and strong correlation of factor scores with the amount of sphalerite and galena, the first association corresponds to the subepithermal silver–base metal ore, whereas the second association corresponds to the intermediate sulfidation gold–silver ore. The positive correlation of the F3 scores with the amount of pyrite, sphalerite, and bornite with not documented rare gold and silver minerals because of their impossible field identification provides indirect evidence for only spatial superposition of the gold–silver mineralization onto the porphyry- and subepitherma-stage ores. However, the composition of this association is completely consistent with the results of an accurate mineralogical study in which the intimate association of low-fineness native gold and hessite was identified (Nagornaya, 2013).

The values of factors average-weighted by the borehole depth were applied to construct the lateral zoning scheme of the Nakhodka ore field.

According to the distribution of geochemical associations, the Nakhodka ore field is characterized by clear concentric zoning (Fig. 8a).

The geochemical structure of the ore field is horseshoe-shaped; its inner part seems to be barren. The internal zone of the anomaly field surrounding the barren space includes an association of ore elements related to the economic ores of the porphyry Cu–Mo stage of the PES evolution, whereas the outer zone includes a geochemical association that corresponds to the Au–pyrite ore.

The associations of the subepithermal (transitional) and epithermal stages are mainly observed in the outer zone, although they are frequently superimposed on the internal zone, especially in the southern part of the ore field.

Plotting of isolines of the AuAgTe/CuMoBiSe × 1000 multiplicative indicator with elements of the epithermal stage in the numerator and elements of the porphyry stage in the denominator provides the best zoned relationships between associations of the major ore types and indicates the localization of epithermal mineralization in the outer "pyrite" area (Fig. 8b).

Table 5. Principal component analyses of geochemical data

Element	Factors					
	F1	F2	F3	F4	F5	F6
Ag	**0.66**	0.15	**0.49**	0.08	0.09	0.09
As	0.08	**0.84**	0.02	0.17	0.15	0.14
Au	**0.26**	0.03	**0.72**	**0.21**	0.04	0.10
Bi	0.07	0.04	0.07	0.08	**0.86**	–0.10
Cd	**0.88**	0.03	0.12	–0.04	0.05	0.00
Cu	–0.07	**0.23**	0.11	0.00	**0.66**	**0.40**
Fe	0.03	0.04	0.06	**0.93**	0.07	–0.09
Mn	**0.72**	–0.01	–0.04	**0.37**	–0.14	–0.07
Mo	0.03	0.03	0.01	–0.09	0.01	**0.93**
Pb	**0.91**	0.06	0.11	–0.04	0.02	0.02
Sb	0.06	**0.89**	0.12	–0.08	0.02	–0.05
Se	0.00	**0.20**	**0.65**	0.00	**0.34**	–0.03
Te	0.11	0.05	**0.90**	–0.03	0.01	–0.02
Zn	**0.94**	0.03	0.05	0.03	0.01	0.02

Significant values of factor loading are boldfaced.

Table 6. Correlation between sulfide content and factor scores by sampling data of drilled core

Mineral	Factor					
	F1	F2	F3	F4	F5	F6
Pyrite	0.06	0.02	**0.16**	**0.24**	0.12	–0.01
Chalcopyrite	–0.05	0.06	0.06	0.01	**0.27**	**0.21**
Bornite	–0.12	–0.03	**0.18**	0.09	**0.28**	0.10
Fahlores	0.07	**0.18**	–0.06	0.08	0.12	0.05
Molybdenite	0.09	–0.02	–0.01	–0.03	0.05	**0.18**
Sphalerite	**0.51**	–0.03	**0.14**	–0.09	0.11	0.05
Galena	**0.37**	0.01	0.01	–0.04	0.07	0.01

Significant correlation coefficients are boldfaced.

High values of this indicator, which provide evidence for precious metal epithermal mineralization, are typical of the southern part of the ore field (Vesenny deposit, southern part of the Pryamoi prospect) and decrease to the north, where the porphyry ore predominates (the high-grade copper stockwork of the III Vesenny prospect).

The largest area of the high multiplicative indicator values stands out in the western part of the horseshoe structure, which results from the predominant subepithermal base metal and epithermal Au–Ag ores of the Vesenny deposit. The porphyry Cu mineralization in this part of the ore field was recently discovered by drilling at a depth of ~200 m below the surface.

Some features evident from studying this object against the background of general concentric zoning

Table 7. Geochemical associations identified by principal component analyses and related minerals in accordance with probable stages of ore deposition

Geochemical association	Related minerals	Porphyry stage	Subepithermal stage	Epithermal stage
F4 Fe (MnAu)	Pyrite			
F6 Mo(Cu)	Chalcopyrite, molybdenite			
F5 BiCu(Se)	Bornite, chalcopyrite			
F2 SbAs(CuSe)	Fahlores			
F1 ZnPbCdMnAg(Au)	Sphalerite, galena			
F3 TeAuSe(Ag)	Bornite, pyrite, sphalerite			

of the geochemical field should be noted, consistent in general with the classic schemes of PES ore–metasomatic zoning (Lowell and Guilbert, 1970). First of all, these are differences in the structure of the western and eastern parts of the anomaly field. As mentioned above, the former is dominated by epithermal associations and high values of the multiplicative zoning indicator, whereas the eastern part is dominated by associations of the porphyry Cu–Mo stage and low values of the multiplicative zoning indicator. This is caused not only by the observed lateral zoning of the anomaly field, but by a different erosion level related to vertical postore movements of individual blocks.

The vertical geochemical zoning was studied for key cross sections within all prospects of the Nakhodka PES and Peschanka deposit. We calculated the average-weighted concentrations of 14 elements by 50-m-thick intervals within key cross sections to determine the precipitation sequence of ore elements and to suggest the criteria for the estimation of the ore erosion level.

With the use of NYu-2 software, in accordance to the methodology elaborated at the Division of Geochemistry of the Geological Faculty of Moscow State University (Solovov et al., 1990), we determined the third-order zoning indicator of AgPbZn/CuBiMo, which decreases monotonically downward.

The AgPbZn/CuBiMo indicator is applicable to estimate the erosion level of the porphyry–epithermal system as a whole. The geochemical association in the numerator is consistent with the composition of subepithermal and Au–Ag epithermal ore on the flanks and above the porphyry copper stockwork (Vesenny deposit); the major ore elements of the porphyry copper stockwork are given in the denominator.

Figure 9 shows the evolution of these indicators along typical cross sections throughout the prospects of the Nakhodka ore field and Peschanka deposit, which correlate with the generalized and formalized model of ore mineralization within the Baimka trend, which was suggested in this study.

The AgPbZn/CuBiMo values have a range of eight orders of magnitude. The minimal values were obtained for the III Vesenny prospect (from $n \times 10^{-3}$ to $n \times 10^{-2}$), where the base metal and Au–Ag ores are the least abundant. The range of intermediate values (from $n \times 10^{-3}$ to $n \times 10^{1}$) was obtained for the Peschanka deposit, which is characterized by subepithermal mineralizarion superimposed on the porphyry copper stockwork and at the Nakhodka and Pryamoi prospects, where late stage geochemical associations occur on the flanks. The maximum values of the indicator ($n \times 10^{1}$ to $n \times 10^{4}$) were obtained for the Vesenny Au–Ag deposit.

The erosion levels of the Nakhodka PES objects and Peschanka deposit estimated from the AgPbZn/CuBiMo zoning indicator are shown in Fig. 10. The Vesenny deposit is shallowly eroded; epithermal ore is completely retained there, and a substantial volume of porphyry copper ore is expected with depth. The stockwork of the Pryamoi prospect is shallowly to intermediately eroded. The Nakhodka prospect and Peschanka deposit are more deeply eroded; their epthermal and subepithermal ores are substantially eroded, and at present, only relics of these ores are found on the flanks of these locations. The most deepely eroded III Vesenny prospect is the least retained porphyry–epithermal system: not only are the features of epithermal and transitional ores not retained here, but judging from the decreasing thickness of orebodies along the dip, porphyry copper ore sharply pinches out downward.

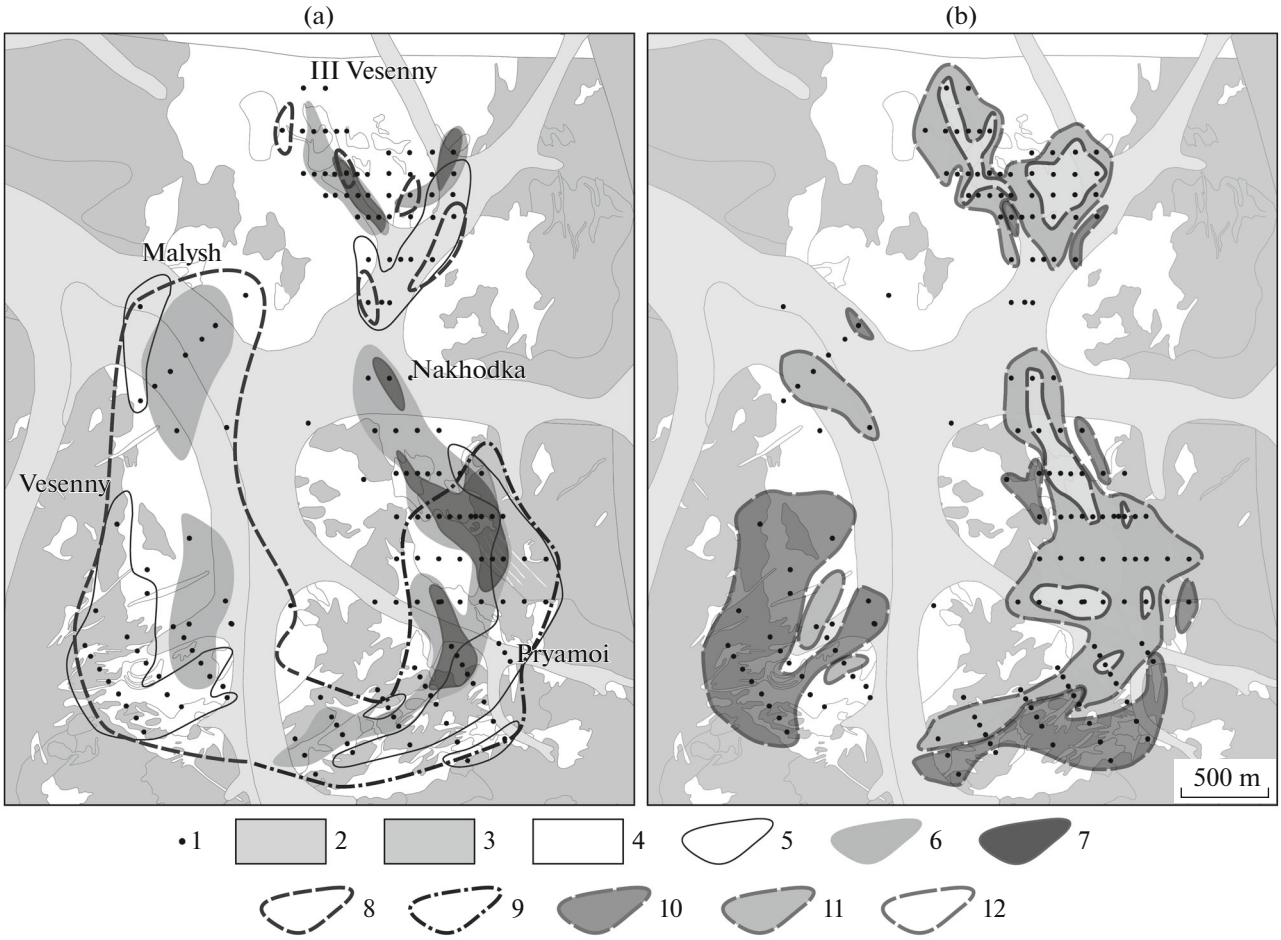

Fig. 8. Structure of Nakhodka PES geochemical field in plan based on (a) data of principal component analyses and (b) multiplicative indicator. (1) Borehole mouths; (2–4) rocks: (2) Quaternary sediments, (3) preore magmatic and postore terrigenous and volcanic rocks, (4) porphyries of Egdygkych Complex with associated porphyry Cu–Mo mineralization; (5–9) areas of geochemical associations and corresponding PES components: (5) Fe(MnAu), pyrite aureoles around ore stockworks, (6) Mo(Cu), porphyry Cu–Mo stockworks, (7) BiCu(Se), rich bornite "cores" of porphyry Cu–Mo stockworks, (8) ZnPbCdMnAg(Au) and TeAuSe(Ag), vein zones with subepithermal Ag–base metal and epithermal Au–Ag mineralization; (9) SbAs(CuSe), fahlores; (10–12) areas of contrasting multiplicative values (AuAgTe/CuMoBiSe) × 1000: (10) high values (>300) typical of areas of precious metal epithermal mineralization, (11) intermediate values (0.1–10) corresponding to porphyry Cu–Mo stockworks, (12) low values (<0.1) recorded in rich bornite "cores" of ore stockworks.

DISCUSSION

The geological, mineralogical, and fluid inclusion data indicate that various ore types within the Baimka trend could be related to various derivatives of the porphyry–epithermal systems. The fluid inclusion study revealed that the fluid regime during the formation of porphyry chalcopyrite–bornite–quartz ore (type I) is typical of porphyry copper–gold deposits, as indicated by the initial high temperature of the ore-forming process, fluid immiscibility, and brine inclusions (Roedder, 1971; Nash, 1976; Eastoe, 1978; Ahmad and Rose, 1980; Klemm et al., 2007). The dolomite–quartz–polysulfide ore (type II) is similar to the subepithermal (transitional) mineralization in the range of homogenization temperatures and salinities of fluid inclusions (Le Fort et al., 2011). The rhodochrosite–high-Mn dolomite–quartz–polysulfide (type III) and quartz–calcite–polysulfide (type IV) ores correspond to epithermal mineralization, whose features were reported by Simmons et al. (2005). The pressure estimated from inclusions of immiscible fluid corresponds to a depth of 0.8–4.4, 1.0–1.7, and about 0.7 km for the formation of porphyry, subepithermal (transitional), and epithermal ores, respectively.

The mineralogical data is evidence that native gold of the Baimka trend is divided into three groups of fineness: high-fineness (917–926), medium-fineness (868–878), and low-fineness and electrum (657–857). The literature data show that the high-fineness gold in the porphyry–epithermal systems is common in porphyry chalcopyrite–bornite and HS epithermal ores (Bogdanov et al., 2005; Bonev et al., 2002; Corbett and Leach, 1998). Since HS epithermal ore are

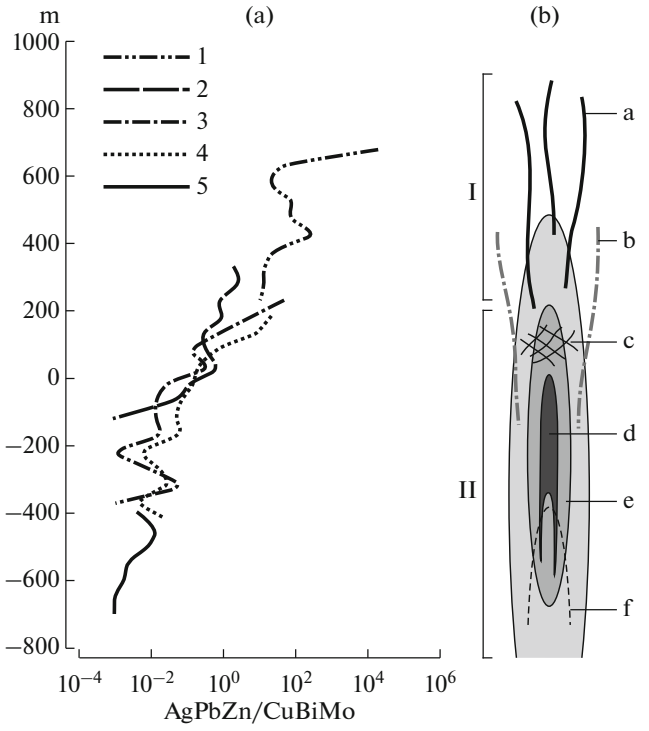

Fig. 9. Variation in AgPbZn/CuBiMo value as indicator of vertical geochemical zoning (a) and geological model of porphyry–epithermal system (b). Conventional depth scale below surface at ore formation is shown. (1–5) Deposits and prospects in Baimka trend: (1) Vesenny, (2) Pryamoi, (3) Nakhodka, (4) Peschanka, (5) III Vesenny. (I, II) Components of porphyry–epithermal system: (I) Au–Ag ore (geochemical association (AuAgPbZnCuAsSbMnTeSe), (II) porphyry Cu–Mo ore (geochemical association CuMoAuBi). (a–f) Main mineral assemblages: (a) Au–Ag epithermal (native gold, hessite, petzite, fahlores), (b) Au–Ag–base-metal subepithermal (sphalerite, galena, chalcopyrite, fahlores), (c) transitional fahlore (tennantite–tetrahedrite), (d) bornite–chalcopyrite, (e) chalcopyrite–molybdenite, (f) molybdenite–chalcopyrite.

absent or eroded at the deposits and prospects of the Baimka trend (Nagornaya, 2013), high-fineness gold cannot be attributed to such a type. However, gold is associated with bornite and chalcopyrite in the absence of other sulfide minerals. This suggests that the high-fineness gold precipitated at the end of the porphyry stage. The medium- and low-fineness native gold and electrum are typical of the carbonate–polysulfide (transitional, subepithermal) stage and IS epithermal stage (Bogdanov et al., 2005; Corbett, Leach, 1998; Carrillo-Rosúa, 2008; LeFort et al., 2011). At the Vesenny deposit, native gold, electrum, and associated galena, sphalerite, fahlores, petzite, hessite, stützite, and acanthite occur in quartz–carbonate veins, in which carbonates are high-Mn dolomite and rhodochrosite (Nagornaya, 2013) attributed to IS epithermal mineralization (Sillitoe and Hedenquist, 2003); therefore, precious mineral mineralization at the deposit is classified as IS epithermal.

The comparatively low fineness of native gold studied at the Peschanka deposit and III Vesenny prospect is caused by its probable belonging to the subepithermal stage of the porphyry–epithermal system, because it is associated with hessite, on the one hand, and high-Mn carbonates are absent in this assemblage, on the other hand.

At the Malysh prospect, gold is associated with hessite, petzite, kurillite, Ag–Te–Se and Ag–Bi–Se phases, and Se-bearing galena to clausthalite. Se-bearing minerals and the absence of high-Mn carbonates prevent attribution of this assemblage to the IS epithermal type. Meanwhile, Se-bearing minerals associated with native gold are typical of both HS and LS epithermal mineralization. Unfortunately, we have no evidence on the relationship of gold and hessite, on the one hand, and Ag- and Se-bearing minerals, on the other hand.

The low-fineness gold + acanthite + naumannite + Se-bearing pearceite + polybasite assemblage found at the Vilka and Pravyi Svetlyi prospects is common to LS epithermal mineralization (Sillitoe and Hedenquist, 2003).

Principal component analyses of the borehole data revealed geochemical associations, making it possible to localize areas of various stages in the porphyry–epithermal system.

The AgPbZn/CuBiMo indicator of vertical geochemical zoning is assumed. The range of this value in inidividual sections of the described locations makes it possible to estimate the erosion level in terms of the porphyry–epithermal system. The Vesenny deposit is shallowly eroded; epithermal ore is completely retained, and a substantial volume of porphyry copper ore at the depth is expected. The Pryamoi prospect is shallowly to intermediately eroded. This series is followed by the Peschanka deposit and Nakhodka prospect, where epithermal and subepithermal ores were substantially eroded and only relics of these ores are found at the locations at present. The porphyry–epithermal system of the III Vesenny prospect is the least retained; it is the most deeply eroded: not only features of epithermal and transitional ores are not retained here, but porphyry copper ore most likely sharply pinches out downward.

CONCLUSIONS

Four types of precious metal mineral assemblages have been established at the deposits and prospects of the Baimka trend. The first type, the chalcopyrite + bornite + quartz assemblage with high-fineness gold enclosed in bornite, terminates the porphyry stage of the porphyry–epithermal system. The second stage, low-M dolomite + quartz + sulfide (chalcopyrite, sphalerite, galena, tennantite–tetrahedrite) ± tourmaline with low-fineness gold and hessite, is attributed to the subepithermal (transitional) stage.

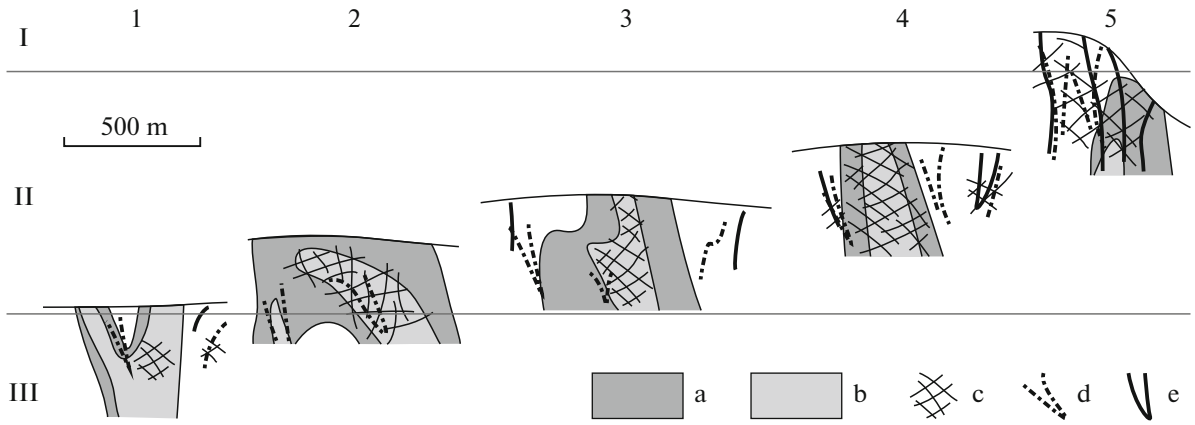

Fig. 10. Erosion level of deposits and prospects in Baimka trend. (I–III) Erosion level: (I) shallow, (II) intermediate, (III) deep. Deposits and prospects: (1) III Vesenny, (2) Peschanka? (3) Nakhodka, (4) Pryamoi, (5) Vesenny (vertical scale for the last deposit is distorted). (a–e) Geological elements of object structure: (a) porphyry Cu–Mo stockwork, (b) high-grade bornite ore, (c) fahlore mineralization, (d) subepithermal polysulfide veins and veinlets, (e) veins with Au–Ag epithermal ore.

Rhodochrosite + high-Mn dolomite + quartz + sulfide (chalcopyrite, sphalerite, galena, tennantite–tetrahedrite) with low-fineness gold, electrum, acanthite, Ag and Au–Ag tellurides, and Ag sulfosalts representing the third type is referred to IS epithermal mineralization. The fourth type, calcite + quartz + sulfide (chalcopyrite, sphalerite, galena) assemblage with low-fine native gold, Ag sulfides and selenides, and Ag-bearing sulfosalts belongs to the LS epithermal mieralization. The study of fluid inclusions from quartz, sphalerite, and fluorite indicates that the ores in the Baimka trend precipitated within a wide range of temperatures (594–104°C) and pressures (1200–170 bar) from aqueous fluids with widely variable salinity. According to the AgPbZn/CuBiMo value, the erosion level of the deposits and prospects of the Baimka trend deepen in the following order: Vesenny deposit → Pryamoi prospect → Nakhodka prospect → Peschanka deposit → III Vesenny prospect.

ACKNOWLEDGMENTS

We are grateful to I.A. Bryzgalov and O.V. Yapaskurt for electron microprobe measurements and O.Yu. Plotinskaya and V.V. Aristov, whose constructive comments significantly improved this paper. This study was supported by the Russian Science Foundation (project 14-17-00170), the Russian Foundation for Basic Research (project no. 14-05-31198a), and the Baimka Mining Company, LLC.

REFERENCES

Ahmad, S.N. and Rose, A.W., Fluid inclusions in porphyry and skarn ore at Santa Rita, New Mexico, *Econ. Geol.,* 1980, vol. 75, pp. 229–250.

Baksheev, I.A., Nikolaev, Yu.N., Prokof'ev, V.Yu., et al., Gold–molybdenum–copper porphyry–epthermal system of the Baim ore zone, Western Chukotka, in *Metallogeniya drevnikh i sovremennykh okeanov-2014. Dvadtsat' let na peredovykh rubezhakh geologii mestorozhdenii poleznykh iskopaemykh* (Metallogeny of Ancient and Modern Oceans-2014. Twenty Years on Frontiers of Geology of Mineral Deposits), Miass: In-t mineralogii UrO RAN, 2014, pp. 108–112.

Bodnar, R.J. and Vityk, M.O., Interpretation of microthermometric data for H_2O–NaCl fluid inclusions, in *Fluid Inclusions in Minerals: Methods and Applications,* Pontignano: Siena, 1994, pp. 117–130.

Bogdanov, K., Filipov, A., and Kehayov, R., Au-Ag-Te-Se minerals in the Elatsite porphyry–copper deposit, Bulgaria, *Bulg. Acad. Scie. Geochem., Mineral., Petrol,* 2005, vol. 43, pp. 13–19.

Bonev, I.K., Kerestedjian, T., Atanassova, R., and Andrew, C.J., Morphogenesis and composition of native gold in the Chelopech volcanic-hosted Au-Cu epithermal deposit, Srednogorie, Bulgaria, *Miner. Deposita,* 2002, vol. 37, pp. 614–629.

Borisenko, A.S., Cryometric study of salt composition of fluid inclusions in minerals, *Geol. Geofiz.,* 1977, no. 8, pp. 16–27.

Borovikov, V.P., *Populyarnoe vvedenie v sovremennyi analiz dannykh v sisteme STATISTICA. Uchebnoe posobie dlya vuzov* (Popular Introduction in the Modern Analysis of data in the STATISTICA System. Tutorial for Higher School), Moscow: Goryachaya liniya - Telekom, 2013.

Brown, P., Flincor: a computer program for the reduction and investigation of fluid inclusion data, *Am. Mineral.,* 1989, vol. 74, pp. 1390–1393.

Carrillo-Rosua, J., Morales-Ruano, S., Morato, D., et al., Mineralogy and geochemistry of El Dorado epithermal gold deposit, El Sauce district, central-northern Chile, *Mineral. Petrol.,* 2008, vol. 92, pp. 341–360.

Chitalin, A.F., Usenko, V.V., and Fomichev, E.V., Baim ore zone–a cluster of large deposits of non-ferrous and precious metals on the western Chukotka, *Mineral. Res. Rossii. Ekonomika i upravlenie,* 2013, no. 6, pp. 68–73.

Chvileva, T.N., Bezsmertnaya, M.S., Spiridonov, E.M., et al., *Spravochnik-opredelitel' rudnykh mineralov v*

otrazhennom svete (Handbook for Determination of Ore Minerals in Reflected Light), Moscow: Nedra, 1988.

Corbett, G.J. and Leach, T.M., Southwest Pacific rim gold-copper systems: structure, alteration and mineralization, *Econ. Geol. Spec. Publ.,* 1998, vol. 6, p. 238.

Eastoe, C.J., A fluid inclusion study of the Pananguna porphyry copper deposit, Bougainville, Papua New Guinea, *Econ. Geol.,* 1978, vol. 73, pp. 721–748.

Kalyuzhnyi, V.A., *Osnovy ucheniya o mineraloobrazuyushchikh flyuidakh* (Principles of the Theory on Mineral-Forming Fluids), Kiev: Naukova dumka, 1982.

Klemm, L.M., Pettke, T., and Heinrich, C.A., Hydrothermal evolution of the El Teniente deposit, Chile: porphyry Cu-Mo ore deposition from low-salinity magmatic fluids, *Econ. Geol.,* 2007, vol. 102, pp. 1021–1045.

Kotova, M.S., Nagornaya, E.V., Anosova, M.O., et al., Dating of metasomatic process and ore-bearing granitoids of copper-porphyry deposits of the Nakhodka ore field (Western Chukotka), in *Geokhronometricheskie izotopnye sistemy, metody ikh izucheniya, khronologiya geologicheskikh protsessov: Mater V Rossiiskoi konf. po izotopnoi geokhronologii* (Geochronometric Isotope Systems, Methods of their Study, and Chronology of Geological Processes. Proceedings of 5th Russian Conference on Isotooe Geochronology), Moscow: IGEM, 2012, pp. 181–184.

Kovalenker, V.A., Plotinskaya, O.Yu., Stanley, C.J., et al., Kurilite–Ag_8Te_3Se–a new mineral from the Prasolovskoe deposit, Kuril islands, Russian Federation, *Mineral. Mag.,* 2010, vol. 74, pp. 463–468.

Kryazhev, S.G., Prokof'ev, V.Yu., and Vasyuta, Yu.V., Application of ICP-MS method for analysis of ore-forming fluids, *Vestn. Mosk. Univ., Ser. 4: Geol.,* 2006, no. 4, pp. 30—36.

LeFort, D., Hanley, J., and Guillong, M., Subepithermal Au-Pd mineralization associated with an alkalic porphyry Cu-Au deposit, Mount Milligan, Quesnel terrane, British Columbia, Canada, *Econ. Geol.,* 2011, vol. 106, pp. 781–808.

Lowell, J.D. and Guilbert, J.M., Lateral and vertical alteration-mineralization zoning in porphyry ore deposits, *Econ. Geol.,* 1970, vol. 65, pp. 373–408.

Moll-Stalcup, E.J., Krogh, T.E., Kamo, S, et al., Geochemistry and U-Pb-geochronology of arc related magmatic rocks, northeastern Russia, *Abstracts with programs GSA*, 1995, vol. 27, no. 5, p. 65.

Nagornaya, E.V., Mineralogiya i zonal'nost' molibden-medno-porfirovogo rudnogo polya Nakhodka, Chukotka. Avtoref, Cand. Sci. (Geolmin) Dissertation, Moscow, 2013.

Nash, J.T., *Fluid-inclusion petrology, Data from Porphyry Copper Deposits and Applications to Explorations,* Washington: US Government Printing Office, 1976.

Pasava, J., Vymazlova, A., Kosler, J., et al., Platinum-group elements in ores from the kalmakyr porphyry Cu–Au–Mo deposit, Uzbekistan: bulk geochemical and laser ablation ICP-MS data, *Miner. Deposita,* 2010, vol. 45, pp. 411–418.

Prokof'ev, V.Yu., Types of hydrothermal ore-forming systems (from fluid inclusion studies), *Geol. Ore Deposits,* 1998, vol. 40, no. 6, pp. 457–470.

Roedder, E., *Fluid Inclusions* in *Rev. Mineral.,* 1984,vol. 12.

Roedder, E., Fluid inclusion studies on the porphyry-type ore deposits at Bingham, Utah, Butte, Montana, and Climax, Colorado, *Econ. Geol.,* 1971, vol. 66, pp. 98–120.

Shapovalov, V.S., Signs of a single OMS by the example of complex formational mineralization, Western Kamchatka, in *Problemy rudno-formatsionnogo analiza i poiskovoi mineralogii na severo-vostoke Rossii* (Problems of the Ore Formation Analysis and Prospecting Mineralogy in Northeast Russia), Magadan: SVKNII DVO RAN, 1994, pp. 73–82.

Shavkunov, B.N., Application of geophysical and geochemical data for outlining ore fields within the Baim gold cluster, in *Geokhimicheskie metody poiskov mestorozhdenii zolota po vtorichnym oreolam rasseyaniya* (Geochemical Exploration for Gold Deposits from Secondary Dispersal Halo), *Zabaikal. Fil. Geograf. O-va SSSR,* 1973, vol. 88, pp. 112–114.

Sillitoe, R.H. and Hedenquist, J.W., Linkages between volcanotectonic settings, ore-fluid compositions, and epithermal precious metal deposits, *Soc. Econ. Geol. Spec. Publ.,* 2003, vol. 10, pp. 315–343.

Sillitoe, R.H., Porphyry copper systems, *Econ. Geol.,* 2010, vol. 105, pp. 3–41.

Simmons, F.A., White, N.C., and John, D.A., Geological characteristics of epithermal precious and base metal deposits, Econ. Geol. 100th Anniversary Vol. 2005. *Soc. Econ. Geol.*, *Inc*. pp. 485–522.

Solovov, A.P., Arkhipov, A.Ya., Bugrov, V.A., et al., *Spravochnik po geokhimicheskim poiskam poleznykh iskopaemykh* (Guidebook on Geochemical Exploration of Mineral Resources), Moscow: Nedra, 1990.

Tarkian, M. and Koopman, G., Platinum-group minerals in the Santo Nomas II (Philex) porphyry copper-gold deposit, Luzon Island, Philippines, *Miner. Deposita,* 1995, vol. 30, pp. 39–47.

Tarkian, M., Hunken, U., Tokmachieva, M., and Bogdanov, K., Precious-metal distribution and fluid-inclusion petrography of the elatsite porphyry copper deposit, bulgaria, *Miner. Deposita,* 2003, vol. 38, pp. 261–281.

Volkov, A.V., Savva, N.E., Sidorov, A.A., et al., Spatial distribution and formation conditions of Au-bearing porphyry Cu–Mo deposits in the Northeast of Russia, *Geol. Ore Deposits,* 2006, vol. 48, no. 6, pp. 448–472.

Translated by I. Baksheev